Chemical Engineering Journal 428 (2022) 132603

Contents lists available at ScienceDirect

Chemical Engineering Journal

journal homepage: www.elsevier.com/locate/cej

Recent advancements, doping strategies and the future perspective of perovskite-based solid oxide fuel cells for energy conversion

Muhammad Bilal Hanif [a,b,*], Martin Motola [b], Sana qayyum [c], Sajid Rauf [d], Azqa khalid [e], Chang-Jiu Li [a], Cheng-Xin Li [a,*]

[a] State Key Laboratory for Mechanical Behavior of Materials, School of Materials Science and Engineering, Xi'an Jiaotong University, Xi'an, Shaanxi, China
[b] Department of Inorganic Chemistry, Faculty of Natural Sciences, Comenius University in Bratislava, 842 15 Bratislava, Slovakia
[c] Department of Chemistry & Chemical Engineering, Lahore University of Management Sciences (LUMS), Pakistan
[d] College of Electronics and Information Engineering, Shenzhen University, Guangdong Province, 518000, China
[e] Department of Chemical Polymer & Composite Material Engineering, University of engineering and technology New campus, Lahore, Pakistan

ARTICLE INFO

Keywords:
Perovskite materials
Energy storage applications
Solid oxide fuel cells
Doping
Design strategies

ABSTRACT

Solid oxide fuel cells (SOFCs) have the potential to be used in energy conversion technology. Most of the studies aimed at modifications of anode concerning various issues such as component degradation, sulfur poisoning, and carbon deposition at high temperatures, hindering its applications at the industrial level. Different perovskite structure-related compounds are discussed in this article, which could be possible electrode materials in SOFCs. Literature also revealed the successful utilization of various cathode materials in a wide range of temperature in which cobalt-based materials exhibits higher conductivity than cobalt-free once. The selection of initial composition, dopants addition in different electrodes with critical challenges inherent to this material family have been assessed herein which play a vital role in enhanced electrochemical performance. The other aim of this review article is to provide some useful recommendations and prospective directions for designing future electrode materials of SOFCs. The review analysis is done based on different processing parameters and their effect on thermal expansion coefficient, electrical conductivity, mechanical and electrochemical properties, etc. In a nutshell, a detailed overview is critically analyzed for energy conversion and storage applications, which can open many gateways towards the advancement of SOFCs.

1. Introduction

The rising threat to the environment due to fossil fuel emission pushes the world to divert its attention towards renewable energy. Fuel cells (FC) have the potential to cope with the present energy demand of the globe because of their efficiency, stability, and wide range of applications, especially in the transport sector. In this regard, fuel cell technology has drawn attention because of its inherent ability to produce electricity with minimal hazardous waste. Additionally, fuel cells can be used in certain applications with strict demands for perilous sources of energy consisting of constant supplies of power, power stations, and distributed grids. All the fuel cells have different reactions at different temperatures, possessing their pros and cons. The major fuel cells are as follows: molten carbonate fuel cell (MCFC), proton exchange membrane fuel cells (PEMFC), alkaline fuel cells (AFC), phosphoric acid fuel cell (PAFC), and solid oxide fuel cell (SOFC) [1-9].

PEMFC are designed to allow the passage of protons through electrolytes assimilated by a polymer membrane. These cells are characterized by high power density and designed to operate at a wide temperature range from 25 to 80 °C. While in PAFC, electrodes are made up of platinum or its alloy, and concentrated phosphoric acid is used as an electrolyte material. These cells are functional at a temperature range of 150–200 °C [10]. MCFC cells possess electrolyte materials comprised of liquid lithium, sodium, or potassium carbonates. Operated optimum temperature is found to be approximately 650 °C at which carbonyl electrolyte shows enhanced conductivity. AFCs operate at temperature ranges from 25 to 80 °C, have substantial applications in space, and are widely used for water and electricity generation. These cells contain an alkaline solution of KOH which serves as an electrolyte. Due to cathodic reactions, these cells show remarkable cell performance. DMFCs contain

* Corresponding authors at: State Key Laboratory for Mechanical Behavior of Materials, School of Materials Science and Engineering, Xi'an Jiaotong University, Xi'an, Shaanxi, China (M.B. Hanif, C.-X. Li).
E-mail addresses: muhammadbilal@stu.xjtu.edu.cn (M. Bilal Hanif), licx@mail.xjtu.edu.cn (C.-X. Li).

https://doi.org/10.1016/j.cej.2021.132603
Received 20 August 2021; Received in revised form 17 September 2021; Accepted 20 September 2021
Available online 23 September 2021

similar electrolytes as used in PEMFCs. Working temperature for DMFCs is lower than other cells, ranging from 50 to 130 °C. A solid oxide fuel cell is an assembly of electrolyte solution and 2 electrodes; one of which is a cathode that produces oxide ions and the other one is anode which helps in speeding up the reaction which in return produces electricity and other by-products [11-15]. The reaction can be stated in Kröger Vink representation as follows. (Equation 1–4).

At the cathode side:

$$V_{\ddot{O}}+2e^{-}+\frac{1}{2}O_2\rightarrow O_O^x \quad (1)$$

At the anode side:

$$O_O^x+H_2\rightarrow V_{\ddot{O}}+2e^{-}+H_2O \quad (2)$$

$$O_O^x+CO\rightarrow 2e^{-}+V_{\ddot{O}}+CO_2 \quad (3)$$

$$(3n+1)O_O^x+C_nH_{2n+2}=(3n+1)V_{\ddot{O}}+nCO_2+(6n+2)e^{-}+(n+1)H_2O \quad (4)$$

Whereas, O_O^x= O_2-ions on a regular O_2-site in the electrolyte lattice, $V_{\ddot{O}}$ = Oxygen vacancies. Fig. 1. illustrates the working principle of SOFCs.

Perovskite materials are represented by general formula as, ABO_3. A in the formula is for large cations while B represents smaller cations having coordination no of 12 and 6 respectively. Large cations may comprise of alkali, alkaline earth metals, rare earth, or other metals whereas, B represents various transition metals. The research of perovskites was initiated by prof. John B. Goodenough as old as 60 years and reported in his autobiographic book named, "Witness to Grace,". Along with a major contribution towards lithium-ion batteries, his research was a masterpiece in the field of perovskite oxide materials. As of yet, perovskite materials serve as an excellent candidate in the field of energy storage and conversion. A history of perovskite materials development is summarized in Fig. 2. In 1838, William Grove an English scientist invented the first fuel cell and named it, "*Grove cell*" or "*wet cell battery*". The operational mechanism for this type of cell was reverse electrolysis of water [16,17]. Those cells were capable of directly converting the chemical energy of the fuel to electricity and heat by combining H_2, CO/H_2 electrochemically. Gaugain and Becquerel experimentally studied and reported the thermoelectric mechanism of fuel cells by establishing the metal contact between glass and porcelain. Furthermore, Buff expanded his research and correlated the thermoelectric force with the galvanic cell's voltage and batteries, comprising of electrodes made up of mercury, zinc amalgam, and various solid metals.

In 1853 Gaugain discovered the solid electrolyte which led to the SOFCs existence. Furthermore, in 1899 Nernst reported the conductivity of 15-mol.% Y_2O_3-doped-ZrO_2 (15YSZ) and found that reported material exhibits higher conductivity values at elevated temperatures as compared to other metal oxide mixtures as described in Fig. 2. In 1905, Haber assembled the fuel cells manipulating porcelain and glass as solid electrolytes while Pt and Au as electrodes. In 1935, Schottky suggested that 15YSZ can serve as an excellent candidate for solid electrolytes [18,19]. Wanger's experimental studies in 1943 revealed that ionic conduction is caused by oxide solid- solutions, while oxygen vacancies can be created by a doping mechanism in the crystal lattice of the host. Warner's studies were further investigated by Baur and Presis in the coming years, fabricating a solid ceramic oxide fuel cell working with YSZ at a temperature of 1000 °C. A couple of experimental studies were reported in literature allied to the utilization of electrolyte material as a thin layer of solid ceramic and various fabrication designs (planer and tubular) for SOFCs for performance enhancement. Blum et. al very well summarized the development progress of SOFC in their studies. Moreover from the 1970 s to 2010, studies and research were focused on lowering the operating temperature of SOFCs to 300 °C by employing nanocomposite (5–10 μm) and thin-film heterolayer electrolytes [20,21].

Moreover, anodic materials used in SOFCs must meet the following requirements; they should be porous, they should have significant chemical and mechanical stability with higher electronic conductivity, and compatibility with other components of SOFCs. Unfortunately, very few metallic or ceramic materials have been reported which meet all of the mentioned criteria. Among these materials, one is the Ni-based cermet that comprehends all these reported properties but certain problems are associated with its application i.e., Ni deposition over electrode because of low resistivity towards coke formation, resulting in

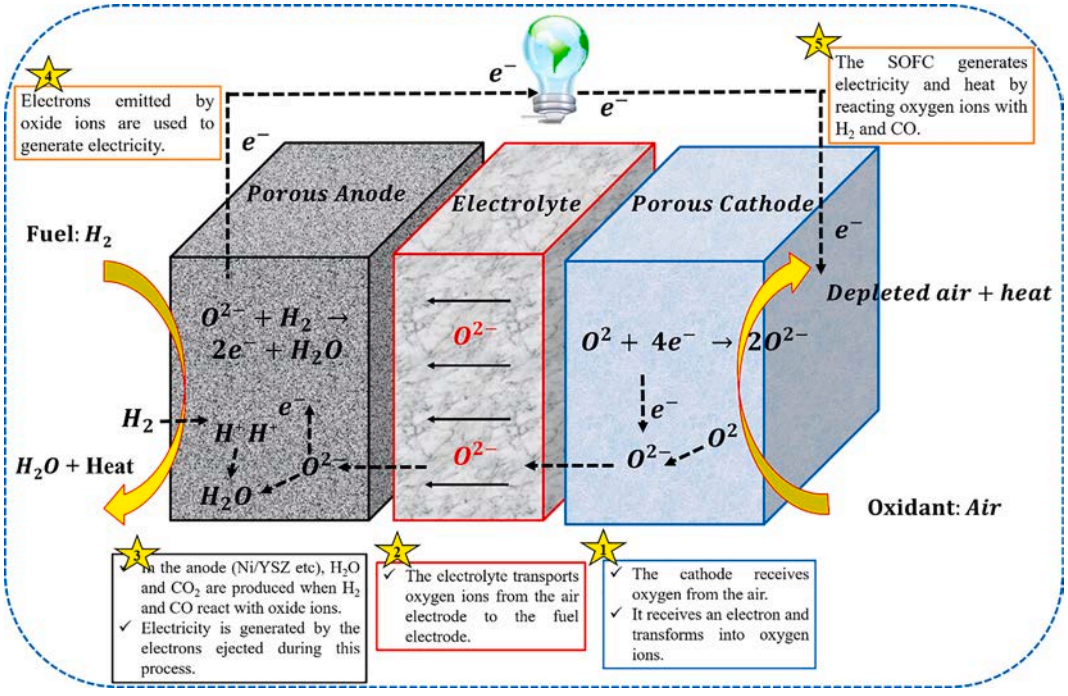

Fig. 1. Working principle of SOFC.

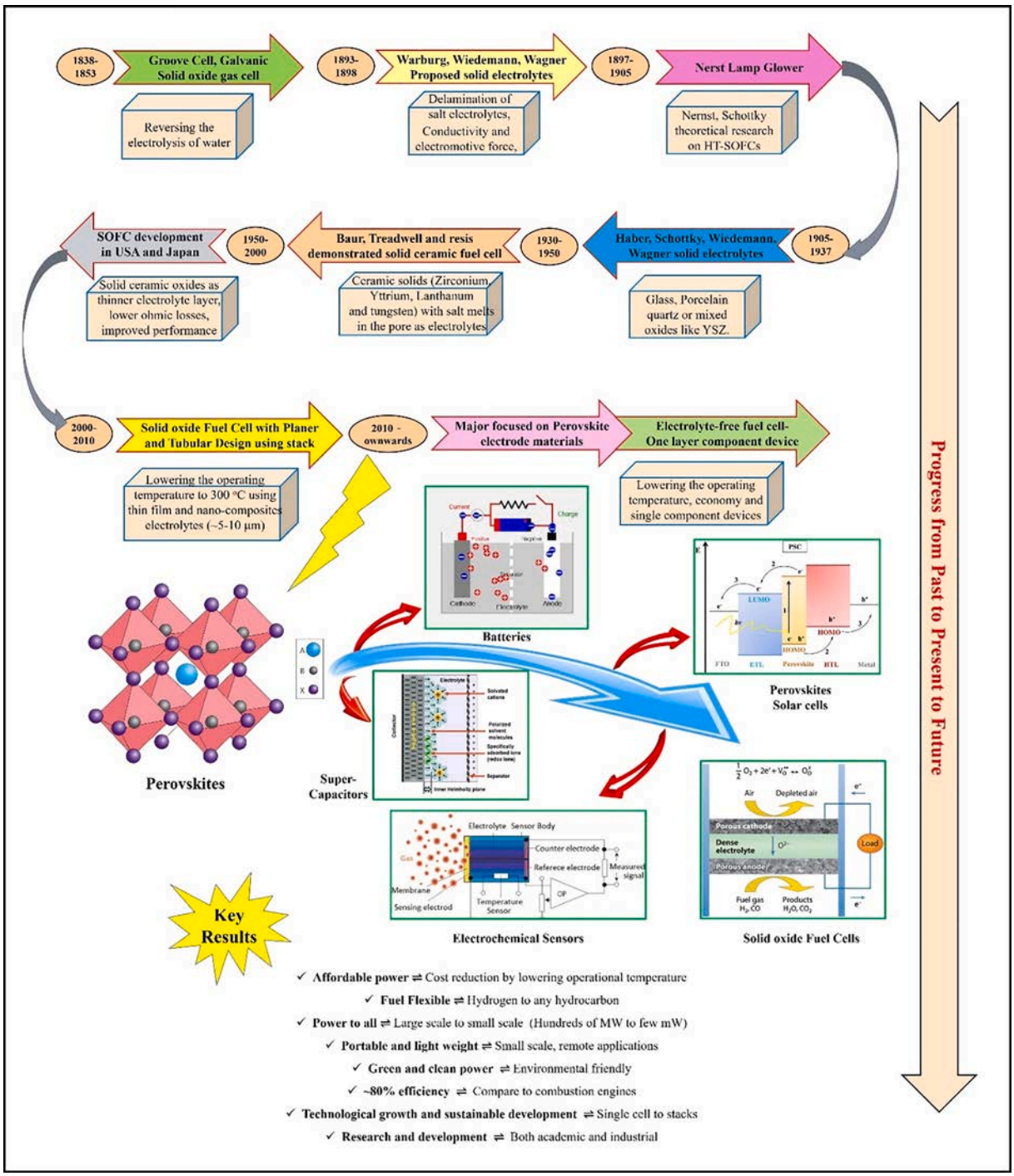

Fig. 2. Trend of energy storage applications for perovskite and SOFC in previous 20 decades.

cell degradation. This suggests that within the search of new fuels, perceptive construction of coking-resistant anode is necessary to commercialize the hydrocarbon-fueled SOFCs. The use of this anodic material is associated with the deposition of carbon generated from hydrocarbon fuel during internal-reforming. Increased oxygen to carbon (O/C) ratio is being utilized as an effective approach (steam/ oxidant) to suppress the formation of coke. However, an increased amount of steam affects the operation stability and efficiency of SOFCs. The only solution to this problem is the utilization of fuel with a high O/C ratio. The major factors associated with the fuel selection include the physical state of fuel (at standard conditions), energy density, cost, and availability. Several publications are currently buckling down to develop several fabrication strategies of anodes, kinetic studies of an anode and, anodic reaction mechanisms for SOFCs [22,23]. However, there is still a need to summarize all the basic features required to develop the anodic materials for SOFCs employing directly oxygenated hydrocarbon fuels.

Material section based on necessity and application plays a significant role in the operational mechanism of the device. Likewise, the selection of materials plays a major role in the functioning of SOFCs. The material must meet several features to be applicable as a cathode. It should possess ionic (10^{-1}-10^{-4} Scm^{-1}) as well as electronic conductivities (>100Scm^{-1}) and compatible coefficient of thermal expansion (CTE) with other modules of SOFC listed as, electrolyte, sealant, and interconnection to eliminate delamination and cracking during

functioning and manufacturing of SOFCs. Porosity is an essential property required (~30–40%) for the diffusion of gases into cathode material for the proper functioning of SOFCs as it is involved in the formation of remarkable gaseous phases of TPB. The performance of SOFCs is substantially affected by the lack of porosity as it is directly concerned with TPB. Porosity is responsible for providing mechanical strength to the thin layer of electrolyte. However, enhanced porosity might be responsible for the reduction of mechanical and electrical properties. In addition, two important parameters are considered for cathode materials including, enhanced catalytic and chemical compatibility of electrolyte and interconnect at the time of fabrication and working. Cathode materials based on lanthanum strontium manganite (LSM) have been reported for significant performance at elevated temperatures (1000 °C). Polarization resistance (Rp) indirectly influenced and increased with decreased operating temperatures for SOFCs because low temperatures (~600 °C) favor the increased activation energy of oxidation–reduction reaction (ORR) making SOFCs (IT-SOFCs) incompatible for intermediate temperature range functioning. Thus, present studies are being focused on the advancement and development of several materials with higher ionic and electronic conductivities for intermediate temperature (600–800 °C) range functioning of SOFCs. But ORR process is dependent on many parameters so it is reported in several publications that the presence of mixed ionic and electronic conducting (MIEC) cathode material is not a standard or an ample condition for reduced Ea of the ORR. Several studies based on the incorporation of dopants to lanthanum and manganese were performed to enhance several properties (mechanical and thermal stability, catalytic activity, and conductivity) of Lanthanum manganite ($LaMnO_3$) systems [24]. Additionally, oxygen vacancies in a system can be enhanced by partially substituting A-site cations with lower valence state cations. Increased oxygen vacancies comprehend the neutrality of the system correspond to higher ionic conductivity and enhanced catalytic properties. According to current studies, oxygen vacancies can be mitigated by substituting smaller ions with lower valences at B-sites so, perovskite materials exhibit higher values of electronic conductivities associated with mixed-valence states of different elements at the B-site [25,26]. However, for the commercialization of SOFCs researchers are being focused on the development of cost-effective materials. So, to overcome the cost factor many, symmetric solid oxide fuel cells have now become significant as these cells are fabricated by using analogous materials as cathode and anode. Implementation of this new conception leads towards many benefits. By swapping the flow of gas, sulfur poisoning and the formation of coke at the anode can be eradicated without any destruction in the cell that enhances the stability and life cycle of fuel cells. The manufacturing process comprises single-step heating due to the identical composition of cathode and anode material [5,27-30].

In this review, recent developments in perovskite cathode and anode materials of solid oxide fuel cells are summarized with prospects. Here, our main purpose is to deliver a brief tutorial corresponding to the structure, properties, and electrochemical behavior of perovskite-based anodes, and cathode in test cells with various dopants together and inherited challenges regarding this material family, which is the novelty of this review article. In addition to this, a perspective has been proposed on the development routes or designs for perovskite oxide-based materials with high performance in energy conversion and storage applications as well as the way forward to cope with the challenges involved in the research route regarding the performance of each component. Perovskite-based materials for Solid oxide fuel cells (SOFCs)

2. Recent advancement of anode materials

The anode is considered as the most imperative component in SOFC where the electrochemical oxidation of fuels takes place. It provides an active electrochemical reaction site and an electron transport pathway. The selection of anode material is an important factor to determine the overall efficiency of the fuel cell. The material chosen for the anode should be of greater electrical conductivity to asses less resistance for transported electrons on a channel. It must also exhibit high carburization and sulfide resistance should be non-reactive towards electrolytes, and ought to retain its higher electro-catalytic activity. The current section gives a detailed overview of different processing parameters and their effect on thermal expansion coefficient, electrical conductivity, mechanical and electrochemical properties, etc. We mainly focused on chromite-based single perovskites, $SrTiO_3$-based perovskites, LST-based perovskites, modified double-perovskites, and their composites in depth.

2.1. Chromite-based single perovskites and their composites

Over the last few decades, numerous research studies have reported that the single perovskites of Sr-doped lanthanum-chromite (LSCr) have been used as anode materials in SOFCs. According to literature, Cr has strong coordination with O_2-deficiency; this is why the cations introduction having lower coordination number can increase the catalytic activity [31]. In reducing atmospheres and at high temperatures, oxygen vacancies can be generated because of the presence of these cations, resulting in improved anode electrical conductivity of LSCr. Irvine and Tao, firstly reported $La_{0.75}Sr_{0.25}Cr_{0.5}Mn_{0.5}O_{3-\delta}$(LSCM) oxygen-deficient perovskite as hydrocarbon-fueled anode material for SOFCs. These materials show compatible electrochemical performance and remarkable catalytic activity at elevated temperatures to traditional Ni/YSZ cermets. Polarization resistance of LSCM in $3\%H_2O/97\%H_2$ was found to be 0.2 Ωcm^2 at 900 °C [21]. However, the two drawbacks of LSCM material were identified as, its low electronic conductivity (σe) in reducing atmosphere as compared to Ni-YSZ cermet and being impotent to abide the poisoning of sulfur impurities present in the fuel.

To improve the electrical conductivity and catalytic activity of LSCr-based single perovskites, four directions have been pursued such as to change the chemical composition of an anode, to make a composite with transition metals having redox activity, to add nanoparticles to make anode composite, and to partially substitute with metal-cations at A or/and B-site. However, the method in which composites with transition metals are prepared has many associated constraints i.e., the preparation is complicated due to the lower melting point of copper and nickel can be deactivated easily by sulfur poisoning. In this section, the studies reported in the literature regarding the dopant and nanoparticles addition on A/B sites of an electrode from doped LSCr will be reviewed.

Mn and Fe co-doping in $La_{0.75}Sr_{0.25}Cr_{0.5-x}Fe_xMn_{0.5}O_{3-\delta}$ ($LSCFM_x$) resulted in enhanced catalytic activity as compared to anodes having either Fe or Mn alone for application involving methane oxidation–reduction. It was anticipated that ionic transport (under reducing environment) and oxygen deficiencies will increase because of the presence of Fe. The measured power density, polarization resistance, and ohmic resistance of $La_{0.75}Sr_{0.25}Cr_{0.3}Fe_{0.2}Mn_{0.5}O_{3-\delta}$ in dry CH_4 at temperature of 750 °C were found to be, 550 $mWcm^{-2}$, 0.48 Ω cm^2, and 0.12 Ωcm^2, respectively [31]. The LSCr-based perovskites have shown rather poor electrical conductivity under a reducing environment (e.g., 6.45 Scm^{-1} for LSCrF and 0.222 Scm^{-1} for LSCrM at a temperature of 800 °C), exhibiting poor electrochemical reaction kinetics in comparison to Ni-YSZ.

Perovskites having a composition of $La_{0.33}Sr_{0.67}Cr_{1-x-y}Fe_xRu_yO_{3-\delta}$(LSCrFeRu) were prepared through solid-state reaction with negligible secondary phase reforming. Instead of adding the Ru nanoparticles separately, they were precipitated onto the anode surface upon heating in a hydrogen environment at the start of operation of SOFC. Upon reduction, the formation of metal nanoparticles was found to be the reason for the improvement of anode's catalytic activity. The introduction of Ru nanoparticles was also effective in reducing the anode polarization resistance. Y. Wan, et al. developed a new methodology to enhance the electrocatalytic performances of $LaCrO_3$-based perovskites. Doping of bismuth at A-site was found to promote performance greater than the

doping of Ru and Pd at B-site. For instance, as shown in Fig. 3(a-d) at a temperature of 800 °C, the 10% doping of bismuth resulted in a 47% increase of peak power density with hydrogen, 85% with ethanol, and 44% with syngas fuel, also 10% decrease in interfacial polarization resistance was achieved.

$$La_{La}^{X} + Cr_{Cr}^{X} \rightarrow Bi_{La}^{\cdot} + Cr_{Cr} \quad (5)$$

$$La_{La}^{X} + Fe_{Fe}^{X} \rightarrow Bi_{La}^{\cdot} + Fe_{Fe}^{\cdot} \quad (6)$$

$$2La_{La}^{X} + O_{O}^{X} \rightarrow 2Bi_{La}^{\cdot} + V_{O}^{\cdot\cdot} + \frac{1}{2}O_2 \quad (7)$$

Fig. 3(e) indicates that nanoparticles used under microscopic characterization are rich in Ru. A peak in the spectrum is also clearly

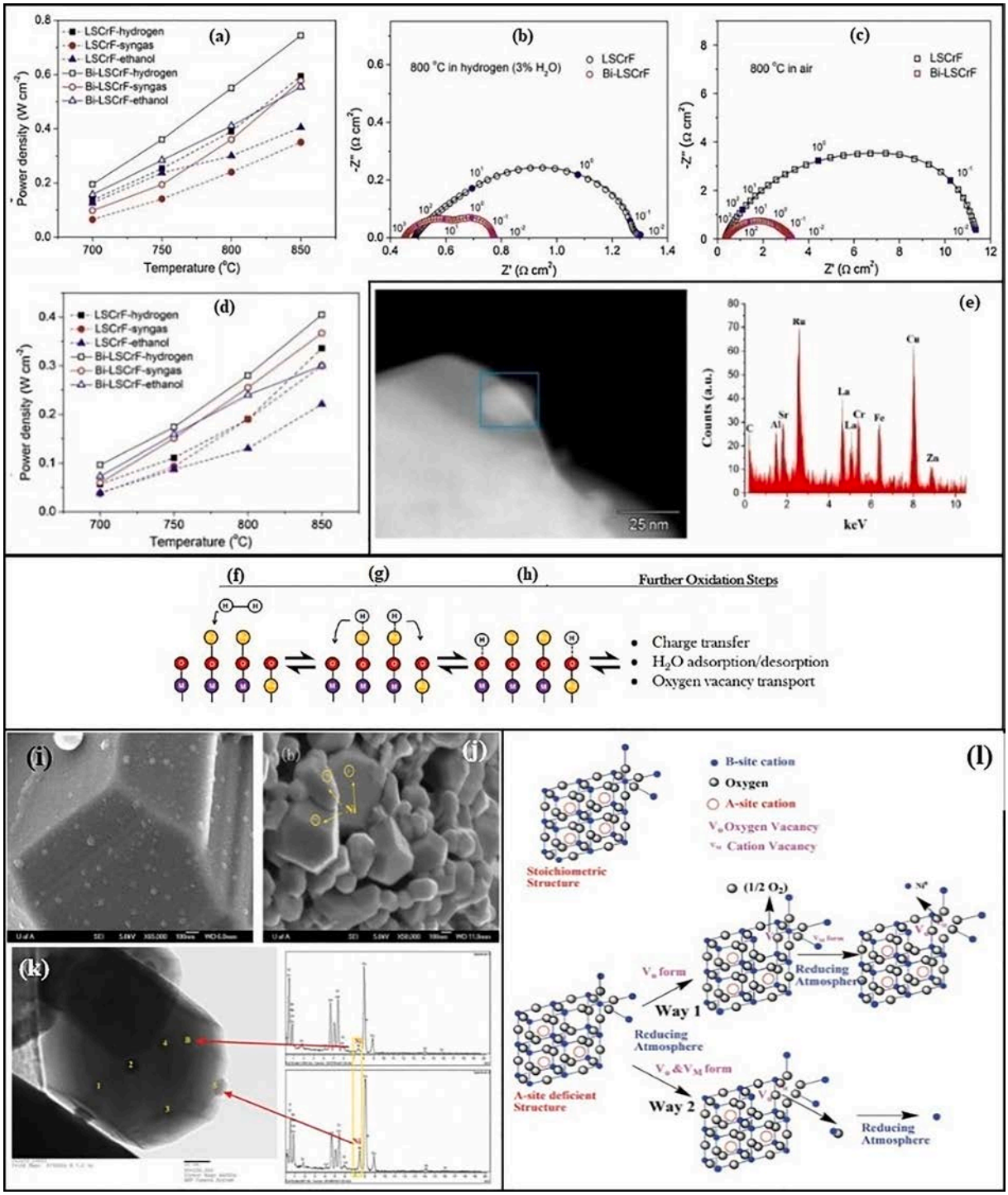

Fig. 3. Peak power densities with different fuels at variable temperatures (a). Nyquist plots of LSCrF and Bi-LSCrF for symmetrical cells determined at a temp. of 800 °C in (b). Humidified hydrogen environment and (c). Air respectively, (d). Peak power densities with different fuels at variable temperatures [32] EDX spectrum, acquired for a section comprising of Ru nanoparticle (e). Schematic of the proposed mechanisms for the hydrogen dissociative adsorption in LSCrF-Ru anodes, containing (f). active dissociation of molecular H_2 by Ru, (g). H atom "spillover" from Ru, and (h). adsorption of H atom onto the oxide surface. [11] SEM images of (i). 63LSCNi-15 and (j). 73LSCNi-15 materials reduced at 800 °C for 4 hrs. While EDX analysis for points 5 and B of the TEM image of 63LSCNi-15 on the left side of (k). The schematic of the generation of oxygen vacancies and the Ni exsolution process for perovskite with A-site deficiency (l).[34].

showing the Fe particles which were substituted on the B-site along with Cr and Ru. Some other spurious peaks can be seen in the spectrum resulting from the carbon present in the support film, copper present in the sample holder and sample grid, zinc present in the sample holder, and aluminum present in the collimator [32]. Fig. 3(f-h). shows the possible mechanism through which Ru assists hydrogen dissociative adsorption. In this model, the presence of Ru particles has increased the adsorption rate resulting in the dissociation of hydrogen gas into adsorbed hydrogen atoms (Fig. 3(f)). As indicated in Fig. 3(g), the produced hydrogen atoms will then spill over onto the oxide surface, which is also observed in the case of other composites of ceramic-metallic material at elevated temperatures [32,33]. Once the hydrogen atoms are adsorbed onto the surface of oxides, the process of the subsequent step is normal (Fig. 3(h)). With the enhancement of adsorption kinetics by the addition of Ru particles, it is presumed that one of the later steps including water desorption, charge transport, and oxygen ion transport becomes the rate-determining [33].

Sun et al. reported in another study that in-situ exsolution of Ni-nanoparticles on Ni-doped LSCr- i.e., $La_{0.6}Sr_{0.3}Cr_{0.85}Ni_{0.15}O_{3-\delta}$ with A-site deficiency shows favorable electrochemical performance along with better redox stability (5000 ppm H_2S-H_2) at a temperature of 800 °C with a maximum current density and power density of >1200 $mWcm^{-2}$ and 460 $mWcm^{-2}$ in comparison with a maximum current and power densities of 300 $mWcm^{-2}$ and 135 $mWcm^{-2}$ respectively for the stoichiometric composition of $La_{0.7}Sr_{0.3}Cr_{0.85}Ni_{0.15}O_{3-\delta}$. Numerous metallic nickel nanoparticles were formed on the A-site deficient

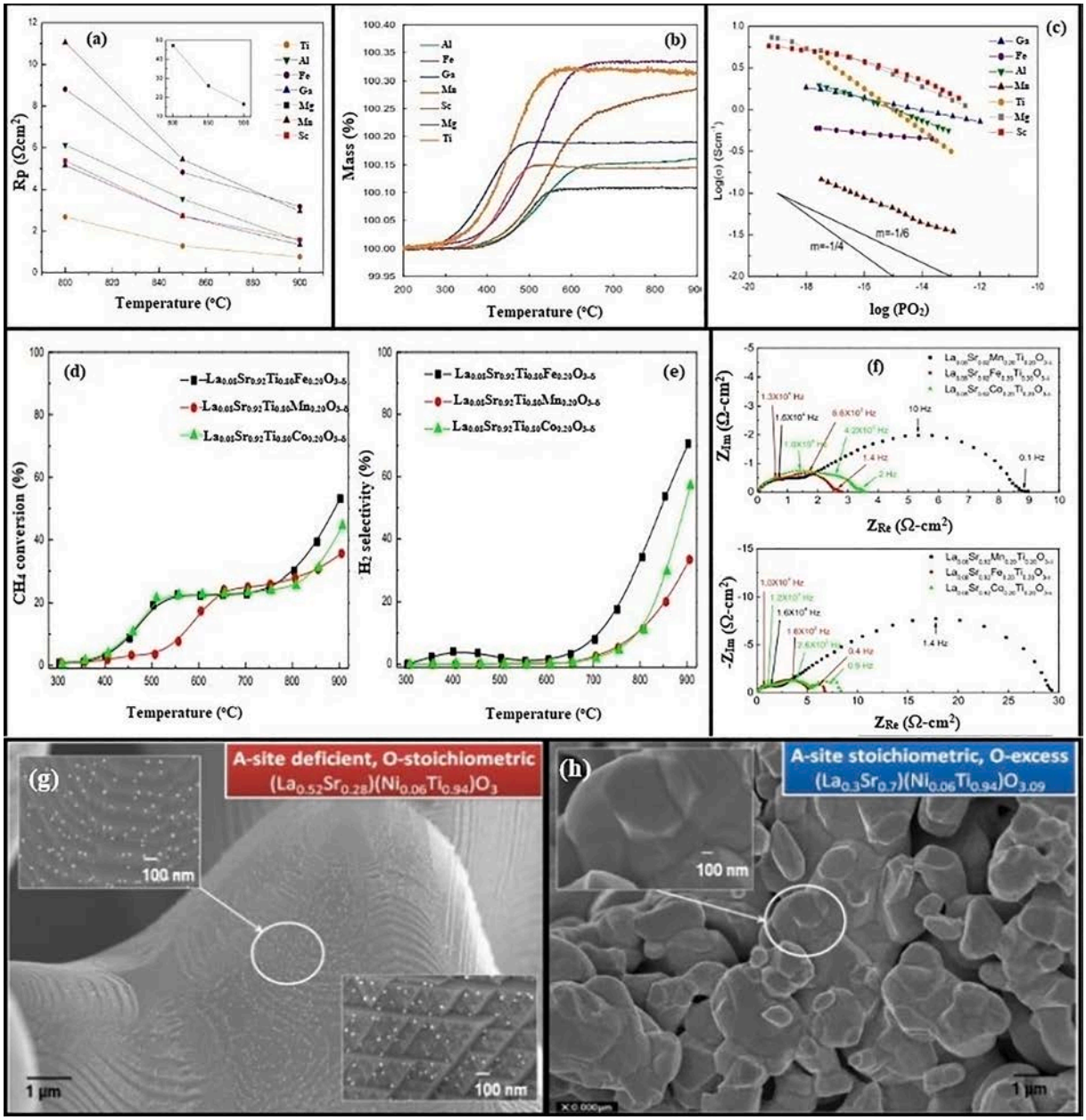

Fig. 4. dependence of polarization with temperature for anodes (LSTX-YSZ) (a). TGA of $La_4Sr_8Ti_{11}XO_{36+\delta}$(X = Ti, Al, Ga, Fe, Mg, Mn or Sc) (b). Change in conductivity of $La_4Sr_8Ti_{11}XO_{36+\delta}$(X = Ti (2), Al, Ga, Fe or Mn) at 870 °C along with partial pressure of oxygen (c) [38]. Rate of methane conversion and hydrogen selectivity for the samples of LSCTO, LSMTO, and LSFTO, (d, e). While (f). illustrate the AC Impedance spectra at 800 °C under wet methane (50%) and wet hydrogen for LSMTO, LSFTO, and LSCTO/ScSZ interface [45]. SEM micrographs illustrating the comparison between the non-stoichiometry formation of exsolutions on stoichiometric and A-site deficient perovskites (g). exsolutions from the initially A-site deficient, O-stoichiometric $La_{0.52}Sr_{0.28}Ni_{0.06}Ti_{0.94}O_3$ after reduction at 930 °C (20 hrs) in 5%H_2/Ar. (h). A-site stoichiometric, O-excess $La_{0.3}Sr_{0.7}Ni_{0.06}Ti_{0.94}O_{3.09}$ samples reduced for 20 hrs at 930 °C with no exsolution [48].

63LSCNi surface after being reduced at the temperature of 800 °C for a total of 4 hrs, whereas, only a few particles were able to be produced in the respective stoichiometric composite [Fig. 4(j)], irrespective of the fact that nickel doping content (15%) was the same in both samples. This indicated clearly that perovskites having A-site deficiency are more prone to B-site species exsolution as compared to the stoichiometric composites. EDX analysis results revealed that the chemical compositions of nanoparticles (point 5) and that of bulk (point B) were different from each other (Fig. 4(k)). The enhanced kinetics of oxygen and hydrogen ions is attributed to the H_2-S-O formation with the absorbed sulfur which explains the stimulating impact of hydrogen sulfide (H_2S). Furthermore, H_2S acts as a carrier of hydrogen, the energy barrier to break the H-S bond (363 kJ mol^{-1}) is lower than that of the H-H bond (436 kJ mol^{-1}) in H_2S which facilitates the reaction, leading to improved anodic performance. For exsolution, two possible processes were hypothesized (Fig. 3(l)). in the first process, because of A-site deficiency, highly mobile oxygen vacancies will be formed, resulting in spontaneous exsolution of nickel nanoparticles and perovskite lattice's instability after reduction. In the second hypothesized process, under a reducing environment, the Ni cation and oxygen vacancies have emerged simultaneously. The catalytic activity and anodic performance were significantly enhanced in A-site deficient LSCNi as compared to stoichiometric LSCNi [34,35].

Cr-based perovskite composites can also be implied to enhance the anode material's performance. To improve electrochemical performance, Zhu et al. impregnated $La_{0.75}Sr_{0.25}Cr_{0.5}Mn_{0.5}O_3$(LSCrM) into the YSZ scaffold. Because of the YSZ phase addition, adhesion was improved and the electrode polarization resistance was reduced of the anodes of LCM/YSZ composites. The primary issue in limiting the electrocatalytic activity of the anode composite (LSCrM/YSZ) is oxygen vacancy diffusion in lanthanum-chromite-based materials. Whereas, in the case of ethanol electro-oxidation reaction the infiltration of palladium nanoparticles greatly improved the anodic activity of LSCrM/YSZ, resulting in eight times increases in the PPD of the cell without any coke formation. By confining the palladium nanoparticles into the nanocages of porous ceria, agglomeration of palladium at elevated temperatures can be effectively overcome which results in stability and enhanced activity of palladium nanoparticles [36].

Before sintering and screen printing as an anode layer, $(La_{0.75}Sr_{0.25})_{0.97}$-$Cr_{0.5}Mn_{0.5}O_3$ with 15 wt% $Ce_{0.9}Gd_{0.1}O_{2-\delta}$ powders were pre-coated using 5 wt% of nickel from nitrates as an anode layer. The GDC-impregnated LSCrM is found to have higher polarization performance than that of the LSCM/YSZ composite and pure LSCM anodes. The nanosized GDC impregnated LSCrM also has greatly improved electrochemical as well as catalytic activities for methane dry reforming. M.K. Rath et al. successfully synthesized $La_{0.75}Sr_{0.25}Cr_{0.5}Mn_{0.5}O_{3-\delta}$-$La_{0.2}Ce_{0.8}O_{2-\delta}$(LSCM-LDC) composite anodes by adjusting different weight ratios of LDC via the sol–gel combustion method. The overall performance increases as LDC acts as a grain growth block agent in LSCM, reducing the electrode's area-specific resistance too. However, in LSCM-LDC composite anodes the deposition rate of carbon increases with the increase in LDC content [37].

2.2. $SrTiO_3$-based single perovskites and their composites

In this portion, we will cover recent studies on $SrTiO_3$(ST)-based perovskites anodes and the addition of various dopants to ST published in the literature till now. It is evident in the literature that $SrTiO_3$ possesses chemical stability in both reducing/oxidizing environments at elevated operating temperatures. Moreover, it has great resistance to carbon and sulfur deposition. However, the conductivity and the catalytic activity of pure-$SrTiO_3$ anode are lower, resulting in higher Rp and lower power density values. Also, it has characteristics of n-type semiconductors along with a wide range of applications. N-type mixed conducting oxides as anode material are preferred as compared to p-type conductors because of their electrical conductivity and structural stability under reducing environments (Equation (8)).

$$2Ti_{Ti}^{X} + O_O^X \rightarrow 2Ti_{Ti}^{\cdot} + V_{\ddot{O}} + \frac{1}{2}O_2 \quad (8)$$

Whereas,

Ti_{Ti}^{X} = tetravalent B-site ion, $Ti_{Ti}^{\cdot}$= trivalent ion, O_O^X = lattice oxygen, $V_{\ddot{O}}$ = oxygen vacancies.

Scientists have explored several ways to boost perovskite conductivity by replacing Ti^{4+} on the B-site and Sr^{2+} on A-site. It involves the production of oxygen that contains sub-stoichiometric compounds which influence the final properties of the product. In addition, various dopants, such as chromium(Cr)[22], gallium(Ga)[25], Scandium(Sc) [31], niobium(Nb)[38], iron(Fe)[39], manganese(Mn)[40], , and on B-site was being investigated. Higher conductivity of 339Scm^{-1} (at 800 °C) has come across with Nb-doped $SrTiO_3$($SrTi_{0.98}Nb_{0.02}O_{3-\delta}$) material. Similarly, due to its better catalytic activity and higher conductivity, the Fe-doped $SrTiO_3$ anode has attracted considerable attention. By reducing Ti^{4+} to Ti^{3+}, lanthanum (La) doped to $SrTiO_3$(LST) at A-site can increase its conductivity and oxygen stoichiometry. Even in the presence of H_2S fuel, LST exhibits reasonable chemical and thermal stability for SOFC under reducing atmosphere. However, its lower catalytic activity for fuel oxidation is not feasible for industrial applications. It showed a peak power density(PPD) of 35 and 1.6 $mWcm^{-2}$ in H_2 and CH_4 at 800 °C respectively [26].

2.3. LST-based single perovskites and their composites

The A or B site dopant properties have shown a great effect on the LST molecule's electrical conductivity, redox, structure, electrocatalytic, and sinterability properties. A series of dopants X (X = Sc^{3+}, Al^{3+},Mg^{2+},Ga^{3+},Fe^{n+},and Mn^{n+}) were studied to find $La_{0.33}Sr_{0.67}$-$Ti_{0.92}X_{0.08}O_{3-\delta}$ anodes by Miller et al. Fig. 4(a) [41-44]. shows the electrical half-cell test results performed in H_2-3%H_2O at a temperature of 900 °C. The $La_{0.33}Sr_{0.67}TiO_{3-\delta}$ had the lowest polarization resistance followed by doped Ga and Sc, followed by doped Mn, Fe, Mg, and Al. As indicated in Fig. 4(c), at oxygen partial pressure of 10^{-18} the conductivities range from 1.5 to 5.5Scm^{-1} of the single valency cation doped X = Mg, Ga, Al, and Sc, undoped X = Ti compounds. As compared to Ga and Al, the conductivities of Mg and Sc are higher because of the experimental design improvements, leading to stronger reducing conditions. When dopant is multivalent Fe (0.15Scm^{-1}) or Mn (0.6 Scm^{-1}) a significant conductivity drop was observed which is attributed to the fact that Mn and Fe-ions get reduced as compared to the Ti-ions as indicated in Fig. 4(b). The use of dopants possesses a great impact on the conductivity and stability of the compounds under oxidizing and reducing atmosphere. It showed variations in conductivity, particle size, and electrochemical performance by enhancing the annealing temperature from 1100 °C to 1300 °C. However, the associated issues with anode material such as degradation and poor long-term stability need to be addressed for successful commercialization.

Suitable doping elements will further increase the oxygen vacancies oxidation state for titanium (i.e., Ti^{4+}/Ti^{3+}). Many catalytic-active elements help to deposit nanoparticles on the surface of LST under reducing conditions. Precipitated nano-particles such as (Fe, Ni, Pd, Co, CeO_2, or Ru) facilitate oxidation reactions for the fuels through the availability of more active sites, which results in enhanced catalytic and electrochemical performance. Furthermore, the amount of exsolved nanoparticles may not be enough to partake in higher catalytic activity. One of the alternative solutions to provide catalytic effect and better ionic conductivity is the introduction of an O^{2-} ionic conductive phase into doped-LST material [39]. Yoon and co-workers studied the doping of Fe, Co, and Mn in $La_{0.08}Sr_{0.92}M_{0.20}Ti_{0.80}O_{3-\delta}$, where (M = Fe, Co, and Mn) and were named as LSFTO, LSCTO and LSMTO respectively [34]. They also studied the effect of perovskite oxide on the catalytic activity of CH_4 fuel through oxidation state and surface atom concentration. In CH_4 fuel, Co and Fe-doped perovskite exhibit higher catalytic activity than

Mn-doped electrode materials, which results in higher oxygen vacancy concentration and higher multivalent redox ratio. This suggests that increased catalytic activity is attributed to a lower oxidation state with a higher concentration of metal ions. Subsequently, ionization of hydrogen or methane can easily be favored by electrons, which revealed that catalytic activity can be enhanced by no. of metal ions comprising of low oxidation states. Since electrons can certainly ionize the molecules. At temperature below 600 °C, the LSFTO methane conversion rate was slightly greater than that of LSCTO, whereas, at above 700 °C the rate was significantly greater. In the case of hydrogen selectivity, a similar trend was observed as presented in Fig. 4(b). As presented in Fig. 4(d-e), the order of enhancement in hydrogen selectivity is LSFTO > LSCTO > LSMTO. However, these materials also showed high resistance to polarization in CH_4 and H_2 atmosphere. At 800 °C, the Rp values of LSFTO, LSCTO, and LSMTO were 2.5, 3.6, and 9.0 Ω cm^2 in H_2, and 7, 8, and 29, Ω cm^2 in 50% Ar/CH_4 respectively as shown in Fig. 5(f). [45]. Rath et al. doped × mol-percent of Ti where (x = 0.2–0.8) and 60 mol-percent of La in $SrTiO_3$, to improve the catalytic activity of $La_{0.08}Sr_{0.92}M_{0.20}Ti_{0.80}O_{3-\delta}$. It has been found that as the Mn content in $La_{0.6}Sr_{0.4}Ti_{1-x}Mn_xO_{3-\delta}$ increases, the ratio of and $Ti^{3+}/Ti^{4+}$and Mn^{3+}/Mn^{4+} also increased. In addition, the Mn-rich anode material $La_{0.6}Sr_{0.4}Ti_{0.2}Mn_{0.8}O_{3-\delta}$ showed the lowest Rp values of (0.011 and 0.054 Ωcm^2) and the highest PPD values of (240 and 290 mWcm^{-2}) at 800 °C in CH_4 and H_2 respectively.

It has been observed that in SOFC anodes, the oxygen vacancies and exsoluted nanoparticles can be created through cation deficiency. Agglomeration of Ni will result in de-percolation, causing particle growth to interrupt electron pathways. This in turn will result in a harmful increase in the ohmic resistance which will significantly reduce the electrochemical activity [45]. The Ni-doped $La_{0.2}Sr_{0.8}Ti_{0.9}Ni_{0.1}O_{3-\delta}$ (LSTN) anode material was prepared by Park and Choi, which was then calcined at 1300 °C for 10 hrs. Nearly half of Ni was observed to be exsoluted from the LSTN surface in H_2 atmosphere at 800 °C for 12 hrs. However, the catalytic activity was comparatively low. Whereas, the PPD and Rp values of the cell LSTN|ScSZ|LSCF-GDC were 150 mWcm^{-2} and 1.66 Ω cm^2 respectively in H_2 atmosphere at 800 °C [46]. Studies suggested that the exsolution of Ni-particles from the surface of electrode material can easily be accomplished by changing the sintering temperature and modifying the fuel atmosphere of LSTN anode material. LSTN was then sintered at 1250 °C in H_2 atmosphere that showed a lower Rp value of (~0.6Ωcm^2) on a cell supported by ScSZ electrolyte. However, the power density of the cell was ~ 130 mWcm^{-2} for 100 hrs at 800 °C under air/H_2 atmosphere respectively. In another research, it has been found that cation deficiency in SOFC anodes can produce oxygen vacancies and exsolved nanoparticles. Recently, a researcher introduced an A-site deficiency on Ni-doped LST anode material (LSNT) to provide an efficient electro-catalytic activity [47]. Fig. 4(g) illustrate the SEM images of A-site deficient (i.e., $La_{0.52}Sr_{0.28}Ni_{0.06}Ti_{0.94}O_3$) and A-site-stoichiometric (i.e., $La_{0.3}Sr_{0.7}Ni_{0.06}Ti_{0.94}O_{3.09}$) perovskite anode material after reducing in 5% H_2/Ar atmosphere at 930 °C. The exsolved Ni nano-particles can be seen homogeneously distributed over the surface of the parent perovskite, while the A-site stochiometric perovskite surface does not facilitate exsolution as shown in Fig. 4(h). Burnat et al.,

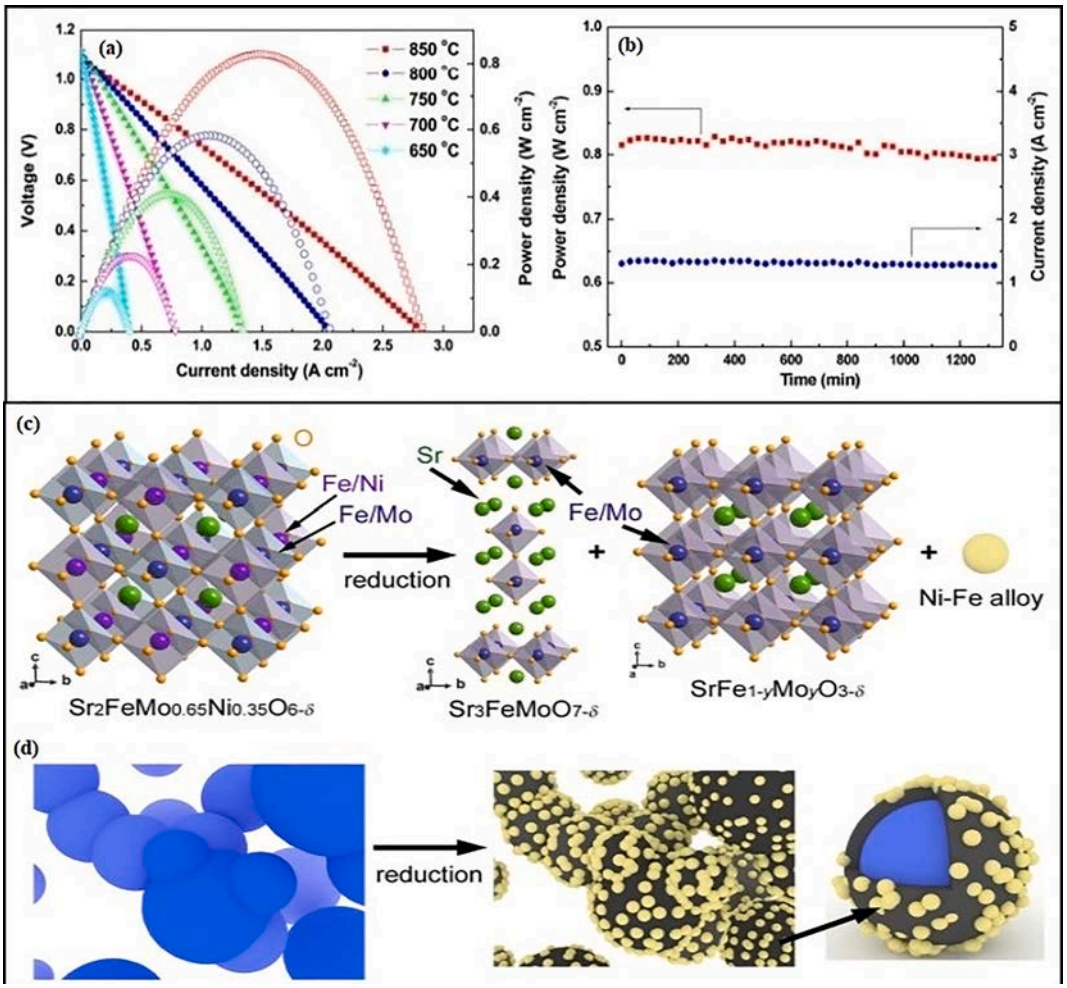

Fig. 5. Illustrate the Power density and cell voltage with variable temperatures under H_2 for $Ba_2FeMoO_{6-\delta}$ (a). Electrochemical stability of a single-cell ($Sr_2FeMoO_{6-\delta}$ anode) under H_2 at 850 °C in (b). [50] Illustration of various models for (c). Structural transformation and (d). $Sr_2FeMo_{0.65}Ni_{0.35}O_{6-\delta}$-anode surface morphology progression in a reduced atmosphere [51].

have studied that, higher deficiencies in A-sites lead towards further Ni exsolution. In addition, the precipitation and recombination of Ni were completely reversible processes during oxidation–reduction reactions. This specified that $La_{0.52}Sr_{0.28}Ni_{0.06}Ti_{0.94}O_3$ exsolved by Ni-nanoparticles was a promising anode material with good catalytic activity and higher electronic conductivity [48].

Chung and co-workers studied the influence of Ru doping nanoparticles on the B-site of LST electrode material i.e., $La_{0.4}Sr_{0.6}Ti_{1-x}Ru_xO_{3-\delta}$(LSTR). Under reducing conditions, trace amounts of Ru metallic nanoparticles were identified on the surface of LSTR which showed a decrease in its electrical conductivity from 343.9 Scm^{-1} for (pure LST) to 202.9 Scm^{-1} for (LSTR0.05) respectively at 900 °C. Ionic conductivity was enhanced from 0.0020 Scm^{-1} (pure LST) to 0.0028 Scm^{-1} for (LSTR0.05) respectively. The main reason for variation in conductivity in B-site deficiency was the production of oxygen vacancies through the reduction of Ti^{3+}. Furthermore, the single-cell anode polarization resistance of LSTR0.05-YSZ was inversely related to time. For example, the Rp value decreased from (4.17 to 2.74 Ω cm^2) after 24 hrs in H_2 atmosphere. While, its PPD increased from 52 $mWcm^{-2}$ (for LST-YSZ) to 115 $mWcm^{-2}$ (for LSTR0.05-YSZ) respectively [49].

2.4. Modified double perovskites and their composites

The double perovskite materials are suggested to synthesize anode with enhanced performance. Numerous cations can be used to substitute A or B or both sites to make different composites. Based on the A and B-site positions, perovskite-type oxides can be either partially or reduced in a reductive environment. Double perovskite materials can be made by substituting the B-site cation ($A_2B_{1-x}B_x'O_6$), the A-site cation ($A_{1-x}A_xB\acute{B}O_6$), or both ($A_{1-x}A_xB_{1-x}B_x'O_6$). In this review, the A and B-site doping on double perovskites anode materials will be reviewed.

$A_2FeMoO_{6-\delta}$ (A = Ca, Sr, Ba) oxides have been investigated as possible double perovskite anode materials for SOFCs. The hybridization and degeneracy of the Fe^{2+}-Mo^{6+} and Fe^{3+}-Mo^{5+} states result in a narrow band formation, which imparts the metallic conduction behavior. The $A_2FeMoO_{6-\delta}$ anodes' electrochemical performance in H_2 is found to be in the order: $Ca_2FeMoO_{6-\delta} < Ba_2FeMoO_{6-\delta} < Sr_2FeMoO_{6-\delta}$ as depicted in Fig. 5(a)[50]. The poor performance in the case of $Ca_2FeMoO_{6-\delta}$ anode was because of its lower oxygen vacancy concentration and its decomposition at elevated temperatures. Whereas, $Sr_2FeMoO_{6-\delta}$ showed a great combination of high thermal stability, electrical conductivity, electrochemical performance, and thermal compatibility, therefore is a potential anode material to be used in SOFCs as illustrated in Fig. 5(b). Yang et al., prepared another anode material with composition of lanthanum-doped $Sr_2FeMoO_{6-\delta}$ ($Sr_{2-x}La_xFeMoO_{6-\delta}$) for SOFCs [51]. Du and co-workers discovered the decomposition of $Sr_2FeMo_{0.65}Ni_{0.35}O_{6-\delta}$ perovskite into Sr_3FeMoO_{7-d}, $FeNi_3$ nano-particle catalyst, and $Sr(Fe,Mo)O_{3-d}$, after reduction as presented in Fig. 5(c). Fig. 5(d) explains under reducing environment the surface morphology of SFMNi. The results reveal that ionic conductivity and oxygen vacancies can be greatly improved by Fe-Ni nanoparticles exsolution, resulting in better performance of anode.

Good-enough and co-workers investigated the nature of $Sr_2Mg_{1-x}Mn_xMoO_{6-\delta}$ anode material by using natural gas (fuel) at 650–1000 °C. Outstanding toughness and sulfur resistance were observed because of variable molybdenum ion [52]. It has great potential because of its higher thermal expansion coefficient, redox stability, and electrocatalytic activity. It is also reported in the literature that Fe-containing $Sr_2Mg_{0.5}Fe_{0.5}MoO_{6-\delta}$ anode for methane combustion gives an improved catalytic activity, the highest conductivity approaching 28 Scm^{-1} in hydrogen at a temperature of 800 °C. The complete substitution of ferric for magnesium (Sr_2FeMoO_6) exhibited higher electronic conductivity (value approaching to 1000 Scm^{-1}) in 5 vol% hydrogen in argon [53].

Huang et al. [54] studied some more members of the Sr_2MMoO_6 series for application as anode materials containing a 3d-block transition metal M (M = Co, Ni). The results revealed that in hydrogen and wet methane, Sr_2CoMoO_6 anode exhibited a higher cell output performance, whereas, Sr_2NiMoO_6 anode showed notable performance only in dry methane. Furthermore, Ji et al., [55] investigated the performances of La-doped $Sr_2NiMoO_{6-\delta}$ ($Sr_{1.2}La_{0.8}MgMoO_{6-\delta}$(SLMM)), where it shows good performance as compared to $Sr_2MgMoO_{6-\delta}$(SMM) for the SOFC which is being operated on moderately desulfurized natural gas at a temperature of 800 C. It can be concluded that double-perovskites can be effectively used as anode material in cells operating on natural gas. Xie et al., reported that the structural stability enhancement of $Sr_2Mg_{1-x}Ni_xMoO_{6-\delta}$(x = 0–0.9) can be achieved up to x = 0.7, suggesting that an increase in nickel doping is attributed to the reduction in the bandgap energy and an increment in the electronic defect's concentration. Equation (9) shows that the creation of oxygen vacancies is accompanied by the reduction Mo^{6+} to Mo^{5+}.

$$2Mo_{Mo}^{x} + O_o^x \rightarrow 2Mo_{Mo}^{\cdot} + V_o^{\cdot\cdot} + \frac{1}{2}O_2 \quad (9)$$

Wang et al. employed a sol–gel process to synthesize $Sr_2MgMo_{1-x}V_xO_{6-\delta}$(SMMV) and studied its potential as an anode for SOFCs that use biogas as a fuel. It was found that $Sr_2MgMo_{0.95}V_{0.05}O_{6-\delta}$ prepared in 5% hydrogen/argon showed better hydrogen-sulfide tolerance, catalytic activity, and stability, for combustion of biogas as compared to SMMO [56]. Further modification by adding metallic nanoparticles can increase the electrical conductivity and catalytic activity for the oxidation of fuel. Li et al. concluded that H_2 adsorption ability and electrical conductivity can be increased gradually by the partially decomposed PBFNO in a reducing environment. Table 1 shows the properties of different perovskite anode materials by varying fuel at different operating temperatures.

3. Recent advancement of cathode materials

A cathode is another main component that affects the SOFC performance. Following are the main requirements for SOFC cathode materials: (a). It should exhibit high electronic conductivity. (b). It should exhibit good compatibility and coefficient of thermal expansion (TEC) equivalent to the electrolyte. (c). It should be of high surface-exchange oxygen kinetics and (d). Resistance to Cr (Chromium) poisoning. The operating temperature can be minimized by applying MIEC (Mixed ionic and electronic conducting) electrodes in SOFC which results in substantial enhancement of three-phase boundary length which further results in increased active sites. The current review article will focus on the defect chemistry, reactivity, electronic structure, stability, conductivity, performance, and surface segregation of lanthanum, Barium, Praseodymium, Neodymium and Samarium, Gadolinium, Yitria, and Strontium-based perovskite cathodes and addition of different dopants for SOFCs.

3.1. Lanthanum, Barium-based perovskites cathode and their composites

$La_{1-x}Sr_xMnO_{3-\delta}$ (LSM) is widely manufactured worldwide and regarded as traditional cathode material. It is attributed to pure electronic conductivity due to which it exhibits remarkable TEC divergence and compatible stability with YSZ electrolyte. However, these cathode materials present some difficulties firstly, at intermediate temperature range (500–800 °C) these materials exhibit increased polarization resistance and secondly interaction between LSM and YSZ electrolyte at elevated operating temperature (>1300 °C) result in lower (less than 30%) Sr- segregation. LSM act as a semi-conductor and its conductivity can be enhanced by doping a p-type impurity that results in increased ionic conductivity of oxide ions [77].

The LSCF perovskite is the most studied and illustrative MIEC cathode material for IT-SOFCs. It has high electrical and ionic conductivities of $1x10^2$ Scm^{-1} and $1x10^{-2}$ Scm^{-1} respectively. Whereas it exhibits a good oxygen surface exchange coefficient (k = $6x10^{-6}$ Scm^{-1}) and

Table 1
List of different perovskite anode materials by varying fuel at different operating temperatures.

Sr. No	Anode composition	Synthesis routes	Conductivity (Scm^{-1}) / Temp (°C)	PPD ($mWcm^{-2}$) /Temp(°C)	EIS ($\Omega\ cm^2$) / Temp	Fuel used	Ref
1	$La_{0.75}Sr_{0.25}Cr_{0.5}Mn_{0.5}O_3$	Solid-state reaction	38/900 °C	470/900 °C	0.2/900 °C	97%H_2/ 3%–H_2O	[57]
2	$La_{0.75}Sr_{0.25}Cr_{0.3}Fe_{0.2}Mn_{0.5}O_{3-\delta}$	Citrate method	1.04/750 °C	550/750 °C	0.48 (H_2), 0.55 (CH_4) / 750 °C	H_2,Dry-CH_4	[58]
3	$SrFe_{0.9}Ti_{0.1}O_{3-\delta}$	Sol-gel method	2.53/600 °C	———	———	5% H_2/Ar	[59]
4	$SrFe_{0.8}Cu_{0.1}Nb_{0.1}O_{3-\delta}$	Sol-gel process,	60/415 °C	423/700 °C	0.25/700 °C	5%H_2/Ar	[60]
5	$La_{0.5}Sr_{0.5}Fe_{0.9}Mo_{0.1}O_{3-\delta}$	Sol–gel method	6.2/800 °C	722(H_2), 513(CH_4) /800 °C	3.04/800 °C	Dry-H_2,CH_4	[61]
6	$Sr_{0.9}Ce_{0.1}Co_{0.2}Fe_{0.8}O_{3-\delta}$	EDTA-citrate method	22/600 °C	150/800 °C	~1.80–1.90 /700 °C	H_2, air	[62]
7	$La_{0.9}Ca_{0.1}Fe_{0.95}Nb_{0.05}O_{3-\delta}$	Citric-acid nitrate method	42.55/850	467.1(H_2), 375.8(CO), / 750 °C	0.75(H_2), 2.30(CO) / 700 °C	H_2, CO	[63]
8	$La_{0.4}Sr_{0.6}TiO_{3-\delta}$	EDTA-citrate method	343.902 /900 °C	52/850 °C	4.95/850 °C	H_2	[64]
9	$La_{0.3}Sr_{0.7}Ti_{0.8}Cr_{0.2}O_3$	Solid-state reaction	53/800 °C	43.86 / 900 °C	———	5% H_2/Ar	[65]
10	$Sr_{0.4}La_{0.6}Ti_{0.8}Mn_{0.2}O_{3-\delta}$	combustion method	2.68/800 °C	290(H_2), 240(CH_4)/800 °C	0.107(H_2) 0.209(CH_4) /800 °C	H_2, CH_4	[66]
11	$Sr_{0.4}La_{0.6}(Fe_{0.75}Ti_{0.25})_{0.6}Ni_{0.4}O_{3-\delta}$	Solid-state reaction	H_2(226), Ethanol(164),NH_3(114), CH_4(89)/600 °C	H_2(318), Ethanol(147), NH_3(226),CH_4(184)/ 600 °C	———	H_2, NH_3, CH_4, Ethanol, NH_3	[67]
12	$Sr_{1.8}La_{0.2}FeMoO_{6-\delta}$	Solid-state reaction	460 /800 °C	885/800 °C	0.35/800 °C	H_2	[68]
13	$Sr_2Mg_{0.5}Fe_{0.5}MoO_{6-\delta}$	Citric-acid nitrate method	28/ 800 °C	———	———	H_2	[69]
14	$Sr_2FeNb_{0.2}Mo_{0.8}O_{6-\delta}$	Solid-state reaction	5.3/800 °C	520 /800 °C	0.057(H_2) /800 °C	H_2, CH_4	[70]
15	$Sr_{1.8}Sm_{0.2}Fe_{1.5}Mo_{0.5}O_6$	Solid-state reaction	25/850 °C	742 /850 °C	0.50 /800 °C	H_2	[71]
16	$Sr_{1.95}Fe_{1.4}Ni_{0.1}Mo_{0.5}O_{6-\delta}$	Combustion method	26.6/800 °C	606 /800 °C	0.48/800 °C	H_2	[72]
17	$Sr_2Fe_{4/3}Mo_{2/3}O_{6-\delta}$	Combustion method	16/800 °C	547/800 °C	0.20/800 °C	H_2 (3%H_2O)	[73]
18	$PrBaMn_2O_5$	Pechini method	8.16/800 °C	1700(H_2) 1300 (propane)	———	5%H_2, propane	[74]
19	$PrBaMn_{1.5}Fe_{0.5}O_{5+\delta}$	EDTA-citrate method	7.4/800 °C	540/800 °C	0.68 /800 °C	5% H_2/Ar	[75]
20	SDC-NiO/$La_{0.6}Sr_{1.4}MnO_{4-\delta}$	EDTA-citrate method	0.69/900 °C	108/800 °C	0.1/700 °C	H_2	[76]

oxygen diffusion properties (D*= $5x10^{-7}$ $S^{-1}cm^{-2}$) at 800 °C, respectively as compared to LSM materials (i.e., k = $5.62x10^{-9}$ Scm^{-1}, D* =$4.0x10^{-15}$ $S^{-1}cm^2$). It has a TEC of 14–15.2x10^{-6} K^{-1}, which is higher than GDC's 11.5–11.9x10^{-6} K^{-1}, but it can be combined with GDC to change the thermal-expansion properties and increase the electrochemical activity [79]. While adding a small amount of doped ceria can improve the surface exchange kinetics and thereby increasing the overall LSCF catalytic activity. Murray et al., [78] demonstrated that adding 50 vol% GDC to LSCF results in a tenfold reduction in polarization resistance, with ASR values as low as 0.01 Ωcm^2 and 0.33 Ωcm^2 at 750 °C and 600 °C respectively for the LSCF/GDC cathodes.

LSCF reacts with zirconia-based electrolytes readily, resulting in secondary phase formation i.e., $SrZrO_3$ at a lower temperature (800 °C). In another study, Chen et al., [79] detected the phase formation of $SrZrO_3$ in the mixture of LSCF-YSZ which is sintered at the temperature of 800 °C for four hours in the air. In contrast to YSZ cubic structure, $SrZrO_3$ possesses an orthorhombic structure at room temperature. The ionic conductivities of $SrZrO_3$ phase, GDC, and YSZ are reported to be 1.87x10^{-6} Scm^{-1}, 8.70x10^{-2} Scm^{-1}, and 5.40x10^{-2} Scm^{-1} at the same temperature values. The development of $SrZrO_3$ as a secondary phase at the cathode/electrolyte interface acts as a blocking layer for O_2-ions and is detrimental to the LSCF cathodes' electrochemical performance [80].

Kindermann et al., [81] explored the $(La_{0.6}Sr_{0.2})_zM_{0.2}Fe_{0.8}O_{3-\delta}$ (M = Cr, Mn, Co, Ni) and YSZ electrolyte compatibility, demonstrating that $SrZrO_3$ is formed when all compositions react with YSZ. The creation of nuclei for the zirconate phase and their consequent rapid growth in the first stage can explain this effect. The reactivity trend of $La_{0.6}Sr_{0.2}M_{0.2}Fe_{0.8}O_{3-\delta}$ with YSZ electrolyte is of the order Mn < Cr > Ni > Co which can be explained by their respective relative stabilities. The A-site substoichiometric, in contrast to LSM, does not affect the activity of $(La_{0.6}Sr_{0.2})_zM_{0.2}Fe_{0.8}O_{3-\delta}$ (M = Co, Ni) perovskite with YSZ. The YSZ and perovskite reaction can be written as shown in Equation (10):

$$SrMO_3 + ZrO_2 = SrZrO_3 + MO_x + \frac{1-x}{2}O_2 \; Where, x = 1 to 1.5 \quad (10)$$

Previously, Lina Miao et al., have reported high-performance Co-free cathode material $La_{1.2}Sr_{0.8}Ni_{0.6}Fe_{0.4}O_{4+\delta}$(LSNF) with $BaZr_{0.1}Ce_{0.7}Y_{0.2}O_{3-\delta}$(BZCY) as an electrolyte. It had low Rp and high conductivity of 0.078 Ωcm^2 and 106 Scm^{-1} at 700 °C respectively [82]. Rongrong Li et al. (2019a), Fangjun Jin et al. developed a potential candidate $La_{1.4}Ca_{0.6}CoMnO_{5+\delta}$(LCCM) for cathode material with the highest ionic conductivity of 223 Scm^{-1} at 800 °C and electrochemical performance of 0.226 Ωcm^2 at 850 °C which was further improved by the addition of $Sm_{0.2}Ce_{0.8}O_{1.9}$(SDC) [83]. Nowadays Co-free perovskite cathodes are considered to be hot research for intermediate temperature SOFCs. Perovskite containing ferrites has attracted more attention as a SOFC electrode due to its excellent electrochemical activity. The materials such as La,Sr(Fe,Mn)$O_{3-\delta}$(LSFM) and $SrFe0.75Mo_{0.25}O_{3-\delta}$(SFM) exhibit high electrochemical properties to be utilized both as cathode and anode. It is well known that (La,Sr)(Co,Fe)O_{3-d} oxides (based on $SrCoO_{3-\delta}$) hold outstanding oxygen transport properties at an operating temperature as higher as > 700 °C [84]. Considering the high redox capacity of LST, researchers have substituted Ti with Co to improve the catalytic activity for oxygen reduction, attributing towards the LST

utilization as a cathode material. However, cobalt-based perovskite, like $La_{0.3}Sr_{0.7}Ti_{1-x}Co_xO$, $La_{0.4}Sr_{0.6}Ti_{1-y}Co_yO_{3-\delta}$, and $La_{2x}Sr_xCoTiO_6$, exhibits high catalytic activity have recently been studied.

Y and Zr co-doped perovskite (BCFZY0.1) are stable, active, and potential cathode for SOFCs working at lower temperatures (≤500 °C). Based on the higher thermal cycling stability, lower activation energy, and higher ORR activity. BCFZY0.1 is suggested to be an intriguing cathode in SOFC applications. To measure its stability, in the long run, cell #1 was operated for>2500 hrs under different operating conditions and no observable performance degradation was observed. J.Felix et al, reported $Ba_{0.5}Sr_{0.5}(Co_{0.7}Fe_{0.3})_{0.6875}W_{0.3125}O_{3-\delta}$(BSCFW) composite consisting of disordered single perovskite and ordered double perovskite oxide phases. Both of these phases interact and promote both chemical and microstructural stability [85,86].

3.2. *Praseodymium, Neodymium and Samarium based perovskites and their composites*

Recently, the double perovskite structures mainly $LnBaCo_2O_{5-\delta}$(whereas Ln = Sm, Pr, and Nd) respectively, have attracted much attention due to faster O_2 exchange on the surface, easier diffusion of O_2 ion, and high electrical conductivity than other simple cathode materials [87]. The high concentration of oxygen vacancies may be available due to increased ORR surface activity and high diffusivity of O^- ions. Ion substitution exhibit some interesting effects on the properties of $LnBaCo_2O_{5-\delta}$ material. For example, it is reported that replacing Pr with Gd can reduce the electrical conductivity, oxygen defects concentration, and performance in a fuel cell. However, the trend of replacing Ba with Sr in the same material is contrary. Researchers have mentioned the synergistic effect of cobalt doping in $LnBaCo_2O_{5-\delta}$ double-perovskite structure, i.e. Sr on (A-site) while Fe on (B-site). It makes different channels for fast diffusion of O_2 ions, and exchange of oxygen surface while maintaining compatibility with IT-SOFC electrolytes.

Despite the good results, the ASR values of $PrBaCo_2O_{5+\delta}$ are not perfectly suitable for cathodic applications when the operating temperature is less than 600 °C. However, the performance can be increased through Sr doping. A simple perovskite $PrBa_{0.94}Co_2O_{5+\delta}$ (SPN-A-PBC) having higher operating stability and electro-catalytic ORR activity was developed by the in-situ exsolving process. At 6 hrs deposition time, the SPN-A-PBC electrode is formed (Fig. 6(d)) which shows a lower Rp (0.025 Ω cm^2) as seen in Fig. 6(c). The single-cell having SPN-A-PBC cathode showed a maximum power density value of 1.1 W cm^{-2} at the temperature of 700 °C (Fig. 6(a-b)). Fig. 6(e) illustrates a possible mechanism of exsolution. At the synthesis temperature of 1050 °C, the

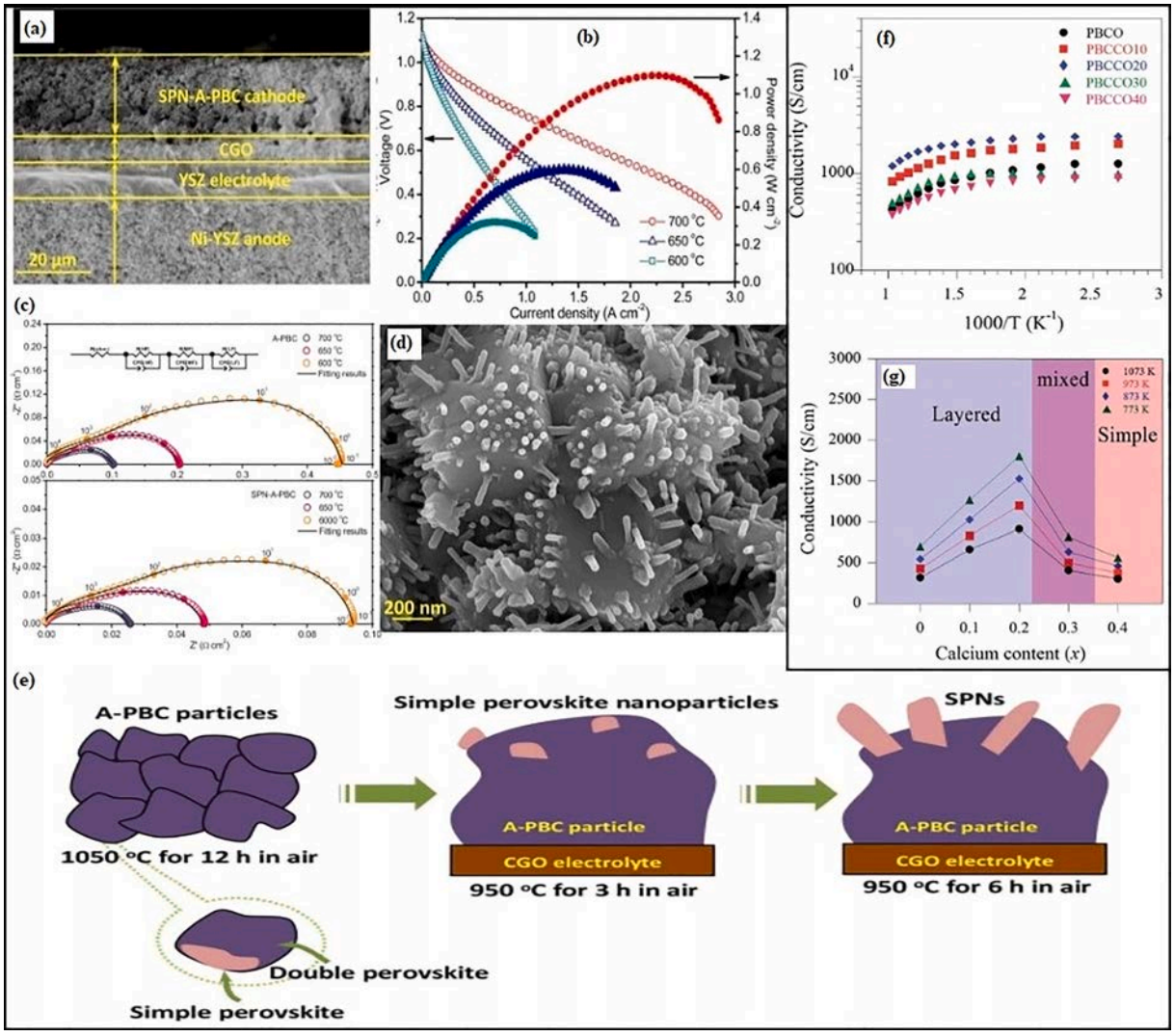

Fig. 6. Cross-sectional illustration of SEM images for the anode-supported single cells (SPN-A-PBC cathodes) (a). and its peak power density at 600–700 °C (b). Impedance spectra of symmetric half-cells with the A-PBC and SPN-A-PBC electrodes at 600–700 °C in the air (c). While its SPN-A-PBC electrode was deposited on a CGO substrate at 950 °C for 6 hrs in the air (d). Schematic for a possible exsolving mechanism of the SPN-A-PBC electrode (e). [88] association between conductivity and Ca doping contents and the electrical conductivity of $PrBa_{1-x}Ca_xCo_2O_{5+\delta}$ and (f, g) [89].

segregation of phases occurred. In the electrode deposition process, the perovskite nanoparticles exsolved and transformed into nanorods [88]. $PrBa_{1-x}Ca_xCo_2O_{5+\delta}$ (PBCC) shows the composition of Ca-doped perovskite which exhibited enhanced electrical conductivity and electrochemical performance with lower thermal expansion. Fig. 6(f) shows the electrical conductivity of the PBCC as described by the Arrhenius plot which decreases with the increase in temperature. Fig. 6(g) shows the electrical conductivity as a function of the amount of calcium, indicating the hole charge carriers are increased because of higher mobile oxygen concentration [89].

Another potential compound is ($PrBa_{0.5}Sr_{0.5}Co_2O_{5+\delta}$), possessing significant conductivity: at the temperature of 600 °C, the conductivity values were increased in the range of 150–900 Scm^{-1} without doping and up to 600–1400 Scm^{-1} with Sr doping. $PrBa_{1-x}Sr_xCo_2O_{5-\delta}$, prepared by Park at al., [90] showed the highest conductivity in the case of Pr-based perovskites. However, as mentioned in the literature these materials are not suitable for cathodic application when accompanied by common electrolytes because of their higher TEC. S. Choiel al., have reported a highly efficient cathode material i.e., $PrBa_{0.5}Sr_{0.5}Co_{2-x}Fe_xO_{5+\delta}$(PBSCF) for LT-SOFC. It was worth notify that when x = 0.5, then the cathode material (named as PBSCF05), exhibits lower Rp values of 0.33 Ωcm^2 and 0.056 Ωcm^2 at 500 °C-600 °C respectively which was almost half of that of BSCF cathode (0.7 Ωcm^2 at 500 °C). Due to a large amount of Fe doping (~50%), the higher oxygen concentration defects in the Ln-O (where Ln = Nd and Pr) layer aid to improve its performance and enhanced oxygen kinetics [91]. Kim et al. synthesized Mn-doped perovskite cathode ($PrBa_{0.5}Sr_{0.5}Co_{2-y}Mn_yO_{5+\delta}$) (y = 0, 0.25, 0.5) and achieved $14.3x10^6$ K^{-1} TEC for $PrBa_{0.5}Sr_{0.5}Co_{1.5}Mn_{0.5}O_{5+\delta}$. By using an anode-supported fuel cell with GDC as an electrolyte, it was found that the composite PBSCF05-GDC as a cathode exhibit an excellent peak density of 2.90, 2.16, 1.31, and 0.71 Wcm^{-2}, under H_2/(3% H_2O) as fuel at 650–500 °C, respectively as compared to BSCF(1.01 Wcm^{-2} at 600 °C) cathode. Ni-GDC|GDC|PBSCF05-GDC cell displays good stability without degradation for 150 hrs under an OCV of 0.6 V at 550 °C [92].

Doping with Nd on the A-site, $Nd_xSr_{1-x}Fe_{0.8}Cu_{0.2}O_{3-\delta}$, is responsible for various factors that affect several electrochemical properties, electrical and thermal expansion. In addition to this, doping significantly affects the structure. Compositions $Nd_{0.5}Sr_{0.5}Fe_{0.8}Cu_{0.2}O_{3-\delta}$ (x = 0.5) are known as, optimum compositions exhibiting an average TEC of 14.7 × 10^{-6} K^{-1} over 25–800 °C with the Rp of 0.071 Ωcm^2 at 700 °C. Studies suggest that there was not any kind of degradation was being observed for the polarization resistance during constant testing for 350 hrs at 700 °C. It was also found that performances of $Nd_xSr_{1-x}Fe_{0.8}Cu_{0.2}O_{3-\delta}$ cathodes are greatly dependent on the availability of surface oxygen vacancy and composition which in turn are dependent on several crystallographic parameters [93].

By Considering Nd as A-site rare earth metal for perovskites, studies reported for Pr-based ones are greater. The $NdBaCo_2O_{5+\delta}$ conductivity values were found to be in a range of 200 to 1000 S cm^{-1} at 600 °C with variable ASR values from 0.2 to 6 Ω cm^2 at the same temperature (600 °C) by up to two orders of magnitudes at 500 °C [94]. Park et al. improved conductivities and ASRs were achieved from the corresponding un-doped perovskites by comparing the electrochemical properties of the perovskite ($NdBa_{0.5}Sr_{0.5}Co_2O_{5+\delta}$) with those reported for Pr-based ones. ASR values ranged from 0.1 to 1.2 Ωcm^2, whereas conductivity values were recorded in the range of 300–2400 Scm^{-1} [95]. Junyu Chen et al., have developed another perovskite material Nd $(Ba_{0.4}Sr_{0.4}Ca_{0.2})Co_{1.6}Fe_{0.4}O_{5+\delta}$ for proton-conducting SOFC which accomplished higher conductivity and low polarization resistance values of 2500 Scm^{-1} at 800 °C and 0.072 Ωcm^2 at 750 °C respectively [96]. Biao Wang et al., have synthesized $Ba_{0.5}Sr_{0.5}Co_{0.8}Fe_{0.1}Ni_{0.1}O_{3-\delta}$ (BSCFN) cathode material which possesses a low Rp value of 0.033 Ωcm^2 at 800 °C and a maximum conductivity of 35.3 Scm^{-1} at 425 °C in air respectively [97]

Although Ni doping is responsible for improved thermal expansion behavior in accordance with ASR and conductivity. Electrochemical performance suffers significantly when doping levels are high. However, by swapping a small quantity of Ni for Co, performance can be improved. According to the literature, $NdBaCo_{1.6}Ni_{0.4}O_{5+\delta}$ is a more promising compound exhibiting $16.9x10^{-6}$ K^{-1} TEC value which is less than the parent compounds. Liu and coauthors [98] reported that lower Cu content causes a decrease in TEC values. However, worsened values were observed for conductivity and ASR containing increased Cu content [95]. $Nd_{0.5}Sr_{0.5}Fe_{0.8}Cu_{0.2}O_{3-\delta}$-$Sm_{0.2}Ce_{0.8}O_{1.9}$ composite cathode with 40 wt% $Sm_{0.2}Ce_{0.8}O_{1.9}$ component showed the compatibility of TEC (13.2×10^{-6} K^{-1}) to $Sm_{0.2}Ce_{0.8}O_{1.9}$ (12.6×10^{-6} K^{-1}). At 700 °C minimum polarization resistance of 0.056 Ωcm^2 was found. The performance of the composite cathode was stable at 700 °C for a time duration of 370 hrs without any considerable change in the polarization resistance performance.

The performance of Sm-doped materials is less studied, but it is found to have some interesting results. The $Sm_{0.6}Sr_{0.4}FeO_{3-\delta}$-$Ce_{0.8}Sm_{0.2}O_{2-\delta}$ cathode was prepared via co-synthesis technique [99]. It showed higher conductivity, enhanced microstructure, and better electrochemical properties as compared to the one prepared via dry-mixing methodology. The comparison of research publications reveals that the interest of researchers is focused on elements presented above and still more work needs to be done to explore the incorporation of elements like Nd, Pr, or Sm in SOFCs application [100].

3.3. Gadolinium, Yttria, and strontium based perovskites and their composites

Compounds having gadolinium in the A site in the form of $GdBaCo_2O_{5+\delta}$ [155] double perovskite were explored by many researchers in the last few years. However, it is seen to be comparatively less efficient. At a temperature of 600 °C, the conductivity is found to be in the range of 100 to 500 Scm^{-1} and the ASR value is between 0.3 and 22 Ωcm^2. By substitution of Sr, a significant improvement is achieved, however, only a few researchers have looked into its electrochemical properties [101,102].

In comparison to $SrFeO_{3-\delta}$ (SF), Xiao et al. discovered that Mo-doping into SF ($SrFe_{1-x}Mo_xO_{3-\delta}$) can maintain the cubic structure in air, enhancing the sintering performance On the other hand, the electrical conductivity was reduced in air. Y increasing the doping ratio to x = 0.25, due to reduction in charged carriers the conductivity value was reduced to 22 Scm^{-1} at a temperature of 800 °C. As indicated in TPR profiles, Mo-doping has improved the tolerance to the reduction of $SrFeO_{3-\delta}$. He et al., studied that tin-doped $Sr_2Fe_{1.5}Mo_{0.5-x}Sn\text{-}xO_{6-\delta}$(SFMSn) positively contribute towards better ORR performance including the bulk diffusion and surface exchange processes. By increasing the tin content from × = 0 to × = 0.3, the re-equilibration time was reduced from 5000 to 600 s, showing that Sn doping can significantly enhance the kinetics of oxygen reduction [103-108]. Mössbauer spectroscopy has revealed that at the larger doping content of Nb, decreasing the Fe^{4+} to Fe^{3+} ratio resulted in a reduction in the average oxidation state of ferric from 3.403 (for $SrNb_{0.05}Fe_{0.95}O_{3-\delta}$) to 3.375 (for $SrNb_{0.1}Fe_{0.9}O_{3-\delta}$) and then to 3.291 (for $SrNb_{0.2}Fe_{0.8}O_{3-\delta}$). Furthermore, the oxygen desorption process and thermal expansion coefficient were also reduced with the increase in Nb content and were explored by Liang and co-workers [108]. Chen et al., has reported a novel cobalt-free Sc-based perovskite cathode having a composition of $SrSc_{0.175}Nb_{0.025}Fe_{0.8}O_{3-\delta}$(SSNF) [109]. It was anticipated that the presence of Nb will enhance the ORR activity and the presence of Sc will restrain the corresponding TEC value.

SC's perovskite structures were typically stabilized/sustained by partial substitution of B-site element with higher oxidation-state elements like phosphorous(P)[110], antimony(Sb)[111], molybdenum (Mo)[112], and niobium (Nb)[113] which contribute to low polarization resistance (R_p) values at low temperatures. Sun and co-workers [156], reported a new promising perovskite cathode material Ce-doped

$SC(Sr_{1-x}Ce_xCoO_{3-\delta})$ which holds good electrochemical performance at an intermediate temperature range. Highly anisotropic displacement factors were observed in $Sr_{0.95}Ce_{0.05}CoO_{3-\delta}$(SCCO) oxygen atoms, suggesting great ionic mobility at 1100 K. Zhou et al., [114] studied an active perovskite cathode material, in addition to single doped-SCs perovskite which was characterized by partial substitution of Co-ions with Nb^{5+} and Sc^{3+}. These dopants result in an exceptionally high ORR activity at a temperature range of 550 °C. Till now, few studies have been reported that co-doping with high-charged dopants may have a synergistic effect on catalyzing the ORR activity in low-temperature SOFC (LT-SOFC) cathodes. They investigated the influence of B-site high-charge dopants on the activity of $SrCo_{0.8}Nb_{0.1}Ta_{0.1}O_{3-\delta}$(SCNT) perovskite cathode materials at low temperatures. These materials showed an excellent and stable electrochemical performance below 500 °C. Symmetric SCNT cathode material displays a low polarization resistance value of 0.68 and 0.16 Ωcm^2 at 450 and 500 °C respectively. Fig. 7(a, b) indicate the peak power density values of SCNT cathode material i.e., 0.7 Wcm^{-2} (at 450 °C) and 1.2 Wcm^{-2} (at 500 °C) respectively. Studies have shown that the substitution of Co for Ta^{5+} and Nb^{5+} will lead to a proper balance of ion mobility, electron transfer, and oxygen vacancies in the surface, which may be beneficial for ORR activity in SCNT cathode [115]. It is reported in the literature that the cubic perovskite structure of $SrFe_{1-x}W_xO_{3-\delta}$ has strong compatibility with SDC electrolyte, whereas $SrFe_{0.7}W_{0.3}O_{3-\delta}$ has the lowest TEC value and is compatible with SDC electrolyte [116]. The high oxidation state W favors the reduction of Fe^{4+} at a lower temperature, resulting in a decrease in formation energy associated with oxygen vacancy Fig. 7(c). Also, by increasing the W content, the temperature associated with the transition from semiconducting to metallic behavior increased. The TEC values of $SrNb_{0.2-x}Ta_xFe_{0.8}O_{3-\delta}$ were closer to that of SDC electrolytes (changed from 13.52 × 10^{-6} K^{-1} to 16.31 × 10^{-6} K^{-1}) as compared to Co-based perovskites i.e., $PrBaCo_2O_{5+\delta}$(20.4 × 10^{-6} K^{-1}) and $Ba_{0.5}Sr_{0.5}Co_{0.8}Fe_{0.2}O_{3-\delta}$ (20.44 × 10^{-6} K^{-1}) at 30 to 850 °C respectively. In another study conducted by Li, Mengran, et al, the 20% tantalum and niobium were substituted into strontium cobaltite's, resulting in $SrCo_{0.8}Ta_{0.2}O_{3-\delta}$(SCT20) and $SrCo_{0.8}Nb_{0.2}O_{3-\delta}$(SCN20) perovskite oxides, respectively. The better performance of the SCT20 cathode was observed as compared to that of SCN20, which is due to the lower electronegativity value of Ta^{5+}. The SCT20 was found to show better ORR performance and less ASR values as compared to SDN20, implying that SCT20 is better for ORR catalyzing. Furthermore, SCT20 cathodes have a lower ORR activation energy than SCN20 cathodes such as 104 and 118 kJ/mol respectively as shown in Fig. 7(d) [117].

In another study, the cathode made up of a commercial $(La_{0.6}Sr_{0.4})_{0.95}Co_{0.2}Fe_{0.8}O_{3-\delta}$(LSCF)-$Ce_{0.8}Gd_{0.2}O_{1.9}$(GDC) composite skeleton and the capping layer of a nano-scaled, ORR-active $SrCo_{0.9}Ta_{0.1}O_{3-\delta}$(SCT). Fig. 7(e) depicts the production of distinct NPs and a constant layer of SCT on LSCF at high and low temperatures. It represents the surface reactions in a Cr-containing environment. In such conditions, the species i.e., CrO_3 (g) will react readily with SrO, resulting in the formation of $SrCrO_4$ which is inactive and insulating, thus ORR active sites are blocked. On the other hand, due to SrO-free surface, SCT will not react with CrO_3(g) [118,119].

Chuangang Yao et al., reported a novel cobalt-free cathode material $SrTa_{0.1}W_{0.1}Fe_{0.8}O_{3-\delta}$ (STWF) which exhibits a lower Rp value of 0.074 Ωcm^2 at 800 °C. However, STWF had lower conductivity of 32.5 Scm^{-1} at 450 °C as Ta and W co-doping leads to Fe^{4+} reduction, thereby regulating the charge neutrality of the crystal. In addition, electrical transfers in STWF samples can damage the Fe^{3+}–O_2-Fe^{4+} network, thereby a drop in the electrical conductivity was observed at high temperatures [120-124]. The performance of cathode material can be improved through surface amendment. Nanoparticles are occasionally

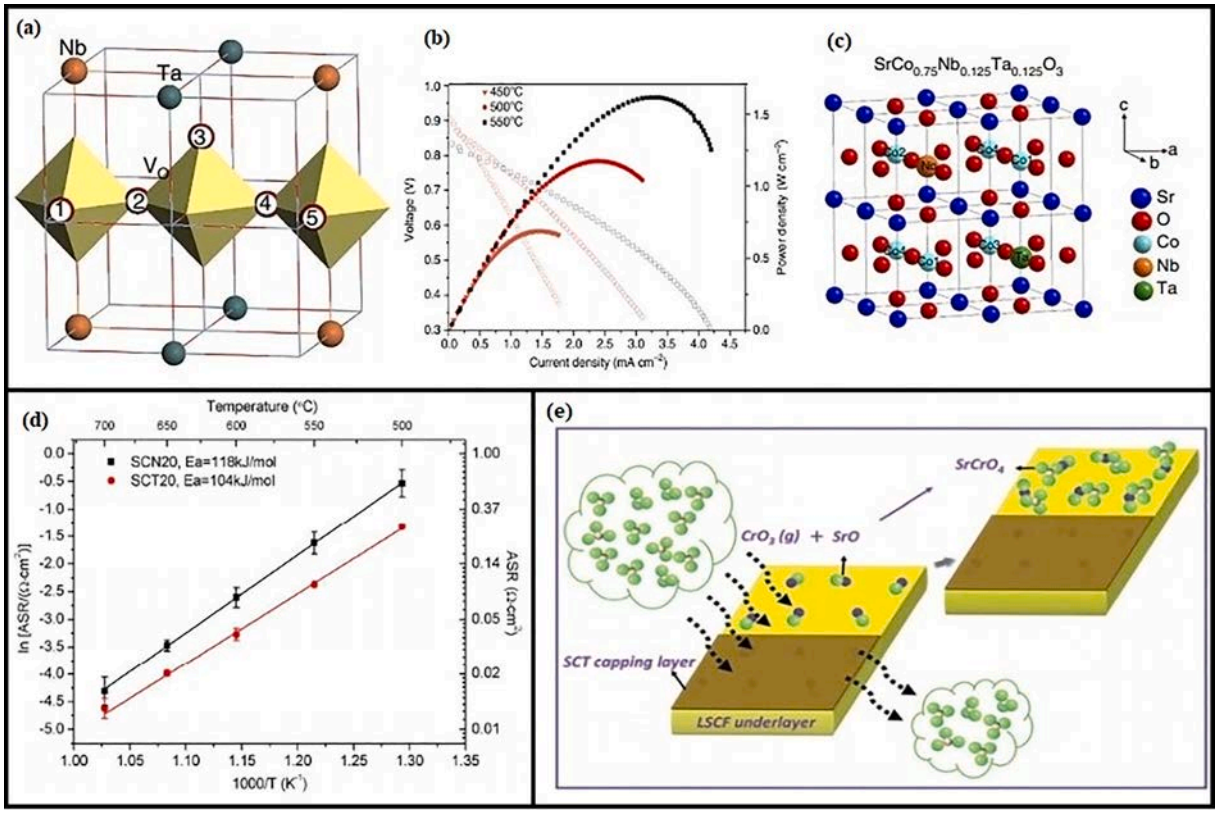

Fig. 7. (a). A diagram showing the minimum energy migration path for oxygen vacancy (V_O) in $SrCo_{0.75}Nb_{0.125}Ta_{0.125}O_{3-\delta}$, where dopants are represented by colorful balls and Co is located within the octahedral along the path. (b). Single-cell performance of anode-supported SCNT | GDC| GDC-Ni at 450–550 °C with air at the cathode and H_2 at the anode. (c). First-principles calculations for the SCNT perovskite oxides, unit cells, single and Co-doped models [117] (d). ORR activation energy of SCT20 and SCN20 cathodes [118] (e). Schematics of infiltrated and untreated cathode depicting chemical tolerant to Cr-species in the air [119].

considered to be very effective for enhancing surface-exchange kinetics. However, due to the high surface energy of nanoparticles, poor thermal stability is a significant problem. Further modifications will help to improve the efficiency of cathode materials. The parameters of various perovskite cathode materials at various operating temperatures are shown in Table 2.

The conductivities and CTE of cobalt-free and cobalt-based materials from distinct references are compared in Fig. 8(a-b) for different operating temperatures.

4. Recent advancement in symmetric perovskite materials and their composites

In previous years, the focus of various studies was performed on different types of materials and it was suggested that there are only a few materials that have been reported as symmetric SOFC electrodes including $La_{0.75}Sr_{0.25}Cr_{0.5}Mn_{0.5}O_{3-\delta}$ (LSCM) [1], $Sr_2Fe_{1.5}Mo_{0.5}O_{6-\delta}$ (SFMO) [2], $PrBaFe_2O_{5+\delta}$ (PBFO) [3], $La_{0.8}Sr_{0.2}Sc_{0.2}Mn_{0.8}O_{3-\delta}$ (LSSM) [4], $Sm_{0.9}Sr_{0.1}Fe_{0.9}Ru_{0.1}O_{3-\delta}$ (SSFR) [5] and $La_{0.5}Sr_{0.5}Co_{0.5}Ti_{0.5}O_{3-\delta}$ (LSCT). These materials are characterized as SOFC but due to various reasons possess limited applications. LSCM exhibits remarkable chemical stability as an anode material in fuel supporting atmosphere with relatively lower electronic conductivity. In addition, LSCM is characterized by poor oxygen reduction activity. These materials show enhanced electrochemical performance at $\geq$ 900 °C used in SSOFC but can be indisputably got poisoned by H_2S [6]. Experimental studies supported by X-ray diffraction suggest that the structure of PBFO materials differs from single to double phase perovskites [7]. Sc and Ru components specified for LSSM and SSFR electrodes are overpriced due which inclusively raises the price of production for SSOFC. Thus, there is a need to develop new symmetric materials having an effective cost of production. Liu et al. have reported a new type of symmetrical perovskite electrode material $Sr_2Fe_{1.5}Mo_{0.5}O_{6-\delta}$ (SFM) with good redox stability, high electronic conductivity in H_2, and air atmosphere for SSOFC. The OCV of the symmetric cell was 1.07 V, using LSGM as an electrolyte under humidified H_2, while the cells OCV ranges to 0.90 V under 3 vol% $H_2O(CH_4)$ as fuel at 900 °C respectively. The PPD of the symmetric SFM were 230 and 835 mWcm^{-2} under CH_4 and H_2 as a fuel at 900 °C. Zhang et al studies revealed that SFHf cathode material exhibit polarization area with low specific resistance value of 0.193 Ωcm^2 at 600 °C for a SFHf|$Sm_{0.2}Ce_{0.8}O_{1.9}$(SDC)|SFHf symmetric cell with highest power density values of 1.94 Wcm^{-2} at 700 °C in anode assisted fuel cell (Ni+$(ZrO_2)_{0.92}(Y_2O_3)_{0.08}$(YSZ)| YSZ|SDC|SFHf) [148].

In another piece of research, $Sm_{0.95}Ce_{0.05}FeO_{3-\delta}$ (SCFO) perovskite-type oxide was evaluated against its potential application as a material of electrode in symmetrical SOFCs. The SCFO was found to have good redox stability when the sample was calcined in 5% H_2/N_2 at a temperature of 850 °C for a total time of 10 hrs. The peak power density when humidified hydrogen was used as fuel at a temperature of 800 °C was as high as 130 mWcm^{-2} [8]. Moreover, $SrFe_{0.75}Zr_{0.25}O_{3-\delta}$

Table 2
Variation in operating temperatures influences the properties of different perovskite cathode materials.

Sr. No	Cathode composition	Synthesis routes	Conductivity (S cm^{-1}) / Temp (°C)	Activation energy Ea (eV)	EIS (Ω cm^2) / Temp	TEC × 10^{-6} (k^{-1})	Ref
1	$La_{0.7}Sr_{0.3}MnO_3$	Combustion method	4.5/1000 °C	0.58	———	11.7	[125]
2	$Pr_{0.6}Sr_{0.4}MnO_{3\pm\delta}$	Combustion method	214/600 °C	———	———	12	[126]
3	$Sm_{0.5}Sr_{0.5}CoO_3$-$La_{0.6}Sr_{0.4}FeO_3$	Pechini method	———	———	0.64/700 °C	17.7	[127]
4	$Sm_{0.5}Sr_{0.5}MnO_3$	Sol-gel method	138/800 °C	13.93 kJmol^{-1}	0.50/800 °C	10.7	[128]
5	$La_{0.6}Sr_{0.4}Fe_{0.8}Ni_{0.2}O_{3-\delta}$	Sol–gel method	130/500 °C	———	0.142/ 800 °C	11.9	[129]
6	$La_{0.8}Sr_{0.2}Co_{0.2}Fe_{0.8}O_{3-\delta}$	Solid-state reaction	41/800 °C	1.684	0.92/800 °C	18	[130]
7	$Ba_{0.5}Sr_{0.5}Co_{0.8}Fe_{0.2}O_3$	Citric-acid nitrate method	37.6/800 °C		0.08/600 °C	20	[131]
8	$Sr_{0.9}Ce_{0.1}Fe_{0.8}Ni_{0.2}O_{3-\delta}$	Smart self-assembly	21.5/650 °C	152.2 kJmol^{-1}	0.028/ 800 °C	16.8	[132]
9	$BaFe_{0.8}Zn_{0.1}Bi_{0.1}O_{3-\delta}$	Citrate combustion method	———	———	———	9.27	[133]
10	$La_{0.6}Sr_{0.4}Fe_{0.9}Nb_{0.1}O_3$	Solid-state reaction	———	———	0.16/800 °C	——	[134]
11	$LaBaFe_{1.925}Nb_{0.075}O_{6-\delta}$	Sol–gel method	101 / 450 °C	0.95	0.056 /800 °C	19.2	[135]
12	$LaBa_{0.5}Sr_{0.5}Fe_2O_{6-\delta}$	Sol–gel method	164.2 /450 °C	1.36	0.152/ 750 °C	18.2	[136]
13	$Ba_{0.95}La_{0.05}Fe_{0.8}Zn_{0.2}O_{3-\delta}$	Sol–gel method	1.9/450 °C	———	2.072/ 750 °C	20.1	[137]
14	$La_{0.6}Sr_{0.4}Fe_{0.9}Ni_{0.1}O_{3-\delta}$	Citric-acid nitrate method	160/400 °C	———	0.14/700 °C	———	[138]
15	$Ba_{0.5}Sr_{0.5}Co_{0.8}Fe_{0.2}O_{3-\delta}$ - $BaZr_{0.1}Ce_{0.7}Y_{0.2}O_{3-\delta}$	Pechini method	———	———	0.10/700 °C	———	[139]
16	$Ba_{0.5}Sr_{0.5}Co_{0.75}Fe_{0.2}Nb_{0.05}O_{3-\delta}$	Citric-acid nitrate method	48/450 °C	———	0.14/700 °C	19.67	[140]
17	$Ba_{0.95}La_{0.05}Fe_{0.85}Cu_{0.15}O_{3-\delta}$	Solid-state reaction	28.25/450 °C	———	0.091/ 700 °C	———	[141]
18	$La_{0.6}Sr_{0.4}Fe_{0.8}Cu_{0.2}O_{3-\delta}$	EDTA-citrate process,	238/575 °C	0.11	0.070/ 800 °C	14.6	[142]
19	$LaFe_{0.8}Cu_{0.2}O_{3-\delta}$	EDTA citrate process,	41.2/800 °C	1.65	0.090/ 800 °C	12.0	[143]
20	$BaFe_{0.8}Cu_{0.2}O_{3-\delta}$	EDTA citrate process,	~9/600 °C	———	———	———	[144]
21	$NdBaCo_2O_{5+\delta}$	Sol-gel method	1000/100 °C	———	0.035/ 700 °C	———	[144]
22	$Sr_2Fe_{1.3}Ti_{0.1}Mo_{0.6}O_{6-\delta}$	Solid state reaction method	220/500 °C	———	0.18/900 °C	13.5	[145]
23	$SrCo_{0.8}Nb_{0.1}Ta_{0.1}O3_{3-\delta}$	Solid state reaction method	~147/400 °C	103.1 ± 0.8 kJ mol^{-1}	0.059/ 550 °C	———	[146]
24	$PrBa_{0.5}Sr_{0.5}Co_{1.5}Fe_{0.5}O_{5-\delta}$	glycine-nitrate process	10–10^3/700 °C	94.75 ± 2.01	0.056/ 600 °C	———	[147]

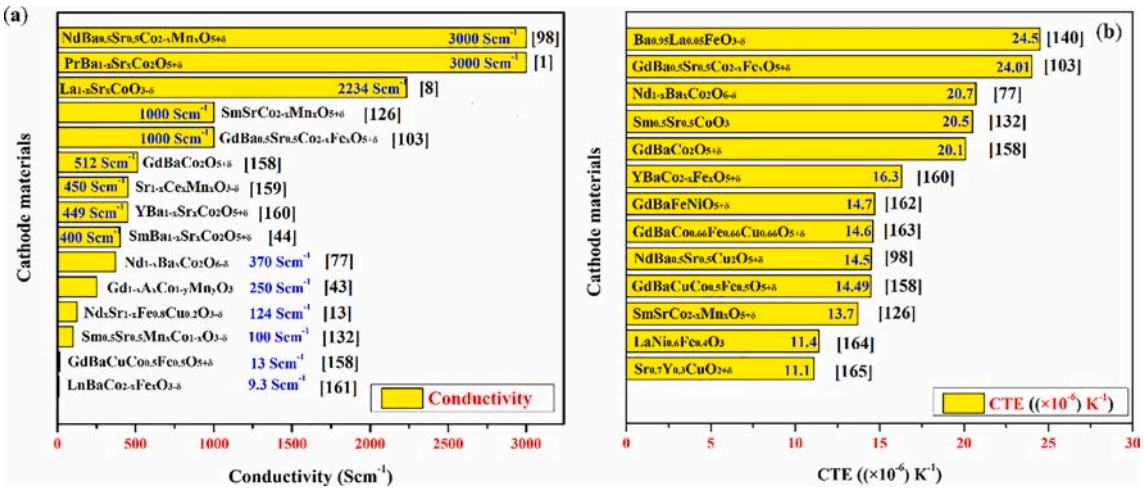

Fig. 8. The best conductivities and CTE values of the cobalt-free and cobalt-based oxides materials evaluated in this review are compared (a, b).

compounds were also assessed about their performance as electrode material in SOFCs. At a temperature of 750 °C, area-specific resistance values as low as 0.17 and 0.1 Ω cm^2 were found in air and 5%H_2-Ar, respectively. A single cell having $La_{0.8}Sr_{0.2}Ga_{0.8}Mg_{0.2}O_{3-\delta}$ (LSGM) electrolyte with 400 μm thickness was used to test the performance of these chemicals as both anode and cathode materials, a maximum PPD value of 425 $mWcm^{-2}$ was achieved at a temperature of 800 °C [149]. The results of x-ray photoelectron spectrometry revealed that niobium doping has significantly increased the Fe-O-Fe (Nb) bind strength as a result after reduction Fe ions can maintain more stabilized oxidation states. The conductivity was also increased from 11.11 Scm^{-1}-15.86 Scm^{-1} in wet-hydrogen and from 17.62 to 27.61 Scm^{-1} in the air because of niobium doping at 600 °C. Moreover, $Sr_2Fe_{1.4}Nb_{0.1}Mo_{0.5}O_{6-\delta}$ also displayed under both reducing-oxidizing conditions, better electrochemical performance in terms of lower polarization resistance. Peak power densities of 531.49 and 364.93 $mWcm^{-2}$ at 800 and 750 °C were achieved in a single symmetrical cell having $Sr_2Fe_{1.4}Nb_{0.1}Mo_{0.5}O_{6-\delta}$ electrode, representing great redox stability [150-154].

Among electrode materials, substances containing nickel and iron are very common and usually have comparable performance. $Ba_{0.5}Sr_{0.5}Co_{0.8}Fe_{0.2}O_{3-\delta}$ (BSCF) [14], $La_{0.8}Sr_{0.2}Cr_{0.5}Fe_{0.5}O_{3-\delta}$ (LSCrF) [15], $La_{0.3}Sr_{0.7}Ti_{0.3}Fe_{0.7}O_{3-\delta}$ [153], $LaNi_{0.6}Fe_{0.4}O_{3-\delta}$ [19], $La_{0.6}Sr_{0.4}Fe_{0.9}Sc_{0.1}O_{3-\delta}$ [20], Ni-$Ce_{0.8}Sm_{0.2}O_{1.9}$(Ni-SDC) [23], $La_{0.3}Sr_{0.7}Fe_{0.7}Cr_{0.3}O_{3-\delta}$ [24] and $SrFe_{0.75}Mo_{0.25}O_{3-\delta}$ [27], as well as the double perovskite structured $Sr_2Fe_{1.5}Mo_{0.5}O_{6-\delta}$ [28] and $Sr_2Co_{1+x}Mo_{1-x}O_6$ [29] showed good performance as compared to LSCF. But their poor stability under the reducing and oxidizing atmosphere is the key problem with these materials. Therefore, by changing the shortcomings of different

Table 3
List of novel symmetric electrode materials by varying fuel at different processing temperatures.

Sr. No	Symmetric electrode material composition	Synthesis routes	Conductivity (S cm^{-1}) /Temp (°C)	PPD ($mWcm^{-2}$) /Temp(°C)	EIS (Ω cm^2) / Temp	Fuel used	Ref
1	$La_{0.8}Sr_{0.2}Sc_{0.2}Mn_{0.8}O_{3-\delta}$	EDTA-citrate method	45 / 850 °C	310, 130 at 900 °C	6.5/850 °C	wet H_2, wet CH_4	[5]
2	$La_{0.75}Sr_{0.25}Cr_{0.5}Mn_{0.5}O_{3-\delta}$	Solid-state reaction	———	546, 347 / 950 °C	0.29/950 °C	H_2, CH_4	[30]
3	$La_{0.4}Sr_{0.6}Co_{0.2}Fe_{0.7}Nb_{0.1}O_{3-\delta}$	Solid-state reaction	———	500 / 850 °C	0.22/850 °C	H_2	[151]
4	$Sr_2Fe_{1.5}Mo_{0.5}O_{6-\delta}$	microwave-assisted combustion method	310 / 780 °C	835, 230 at 850 °C	0.21/850 °C	wet H_2, wet CH_4	[3]
5	$SmBaMn_2O_{5+\delta}$	Citric-acid nitrate method	10.7/900 °C	782/900 °C	0.313/ 900 °C	H_2	[75]
6	La_2NiO_4-infiltrated LSGM	Solid-state reaction	———	520/800 °C	———	H_2	[43]
7	$La_{0.3}Sr_{0.7}Ti_{0.3}Fe_{0.7}O_{3-\delta}$	Solid-state reaction	———	74/900 °C	0.04/900 °C	H_2	[44]
8	$La_{0.2}Cu_{0.4}Sr_{0.4}$	Sol-gel method	~4.70/650 °C	~782/600 °C	———	H_2	[103]
9	$La_{0.7}Sr_{0.3}Ti_{0.1}Fe_{0.6}Ni_{0.3}O_{3-\delta}$	Pechni method	~1.1 / 700 °C	~402/800 °C	0.201/ 800 °C	Dry H_2	[104,152]
10	$LaSr_2Fe_2CrO_{9-\delta}$	Citric-acid Sol-gel method	0.16/800 °C	224/800 °C	0.454/ 800 °C	H_2	[105]
11	$La_{0.6}Sr_{1.4}MnO_4$	Citric-acid nitrate method	0.4/800 °C	59/800 °C	2.07/800 °C	H_2	[106]
12	$La_{0.5}Sr_{0.5}Co_{0.5}Ti_{0.5}O_{3-\delta}$	Citric-acid nitrate method	0.11/900 °C	500/850 °C	———	H_2	[107]
13	$SrFe_{0.8}W_{0.2}O_{3-\delta}$	Pechini method	1.16/850 °C	931/850 °C	0.20/800 °C	H_2	[120]
14	$Sr_2TiFe_{0.9}Mo_{0.1}O_{6-\delta}$	EDTA-citrate method	1.2/500 °C	573, 361 /850 °C	0.237 / 850 °C	H_2, H_2S	[121]
15	$Pr_{0.6}Sr_{0.4}Fe_{0.7}Ni_{0.2}Mo_{0.1}O_{3-\delta}$	EDTA-citrate method	70.1/700 °C / air	500/800 °C	0.07/800 °C	H_2	[122]
16	$Sm_{0.5}Sr_{0.5}FeO_{3-\delta}$	EDTA-citrate method	0.19/750 °C	109.09 /750 °C	4.32/750 °C	H_2	[103]
17	$Sm_{0.5}Sr_{0.5}FeO_{3-\delta}$- $Gd_{0.1}Ce_{0.9}O_{2-\delta}$	EDTA-citrate method	———	201.74 /750 °C	0.91/750 °C	H_2	[123]
18	$BaZr_{0.1}Co_{0.4}Fe_{0.4}Y_{0.1}O_3$-SDC	sol–gel method	———	114.8 /750 °C	0.32 / 750 °C	H_2	[124]
19	$Pr_{0.4}Sr_{0.6}Co_{0.3}$ $Fe_{0.6}Nb_{0.1}O_{3-\delta}$	Solid-state reaction	258.9/ ~600 °C / air	891 / 900 °C	0.077 / 900 °C	H_2	[3]

electrode materials, researchers have synthesized a new type of symmetric electrode material in the future. Table 3 shows the novel symmetric electrode materials with variable fuels at different operating temperatures.

5. Future perspective and concluding remarks

Perovskite materials fall under the category of a most important class of materials and attracted the attention of enormous researchers as functional materials in the fields of energy conversion and storage. Their use has been extensively exploited in the fields of oxy-fuel combustors, fuel cells, batteries, and solar cells. However, on a commercial scale perovskite-based energy storage and conversion devices still not available. Although, in various energy-related fields perovskite materials can find widespread applications in commercially available devices by improving critical performance parameters to some extent. In the past few years, doping strategies encompassing the A-site, B-site, or combined A and B-site doping have remarkably increased the O_2 permeation fluxes of oxide-based perovskite materials. Therefore, offering a big challenge for the development of perovskite materials possessing favorable mechanical strength, chemical stability, and permeability concurrently [120-124]. For instance, cobalt-based perovskite oxides are characterized for higher values of oxygen permeability corresponding to ease of reduction of cobalt ions under reduced atmospheric conditions [84]. Moreover, the A-site of the perovskite structure is doped by the huge amount of alkaline earth metal elements for the introduction of high oxygen permeation flux. However, rare earth elements are receptive towards CO_2 poisoning therefore, a rapid degradation occurs for oxygen permeation within the time as briefly mentioned in Fig. 9 [57-76,125-147].

Cathode plays an essential role to define the electrochemical performance of SOFC. Operational temperature can be minimized by adopting MICE electrodes in SOFC which facilitate the staggering increase in the length of three-phase boundary length which further correspond to increased active sites. Literature survey suggests that the development of cathode materials with elevated properties for a wider range of temperatures is one of the much-concerned issues [87]. Alkaline earth metals are susceptible to poisoning which is a major reported issue in the commercialization of SOFCs so, the introduction of several strategies for the formation of alkaline metal-free perovskite material is another emerging challenge now. Significant conductivity values have been reported for cobalt-based materials but only a few comparative studies have been conducted between cobalt-based and cobalt-free materials. According to high priority needs, cobalt-free particles must be developed to enhance the performance of SOFC with enhanced conductive character. Several parameters (selection of dopant, tuned conditions) must be high priority conditions for the development of highly conductive materials [109]. Mixed conductivities correspond to electronic, protonic, and oxygen-ionic conductivities that can remarkably affect the triple-phase boundary (TPB) length therefore, they represent a consequential R&D handling in the future. Literature survey revealed that mechanical properties of cathode materials have not been studied well, whereas these properties have a significant role as well in the fabrication route of SOFCs. The fuel-testing parameter is considered as one of the versatile parameters to check the durability and stability of materials. Deep understanding regarding the properties and structure relations is necessary for the development of materials, and design strategies with tailored properties for breakthrough applications of perovskites in energy storage and conversion domains in near future. There is a need to yield a cost-effective metal rather than high-priced metals to develop a promising cost-effective symmetrical cathode material [104-107].

In addition to this precedence, symmetrical SOFCs are susceptible to sulphur poisoning and mediated coking and the scientific community is addressing these issues with high priority. Furthermore, oxide-based symmetrical electrodes must have a variable oxidation state at their B-site, as this may encourage partial reduction to a lower oxidation state when exposed to fuel gas, resulting in lattice expansion. Therefore, oxide electrodes might be able to experience several lattice expansions in different environments (cathode and anode) resulting in the induction of large internal strain during redox cycling [5,30,31]. Hence, the criteria of single and stable phase structure under both reducing and oxidizing atmospheres would not be a better criterion for further advancement and development of electrode materials for symmetrical SOFCs. Electrode performance for SOFC is determined by considering the intrinsic properties, microstructure, morphology, and design of the electrode. In most cases, morphology is considered as a prominent parameter for the determination of electro-catalytic activity for ORR and a proper understanding of the operational activity of fuel cells. It has been observed that the scientific community has been focusing on 3D microstructural reconstruction and optimization of electrode materials. Observations revealed that the symmetrical cell configuration of SOFC can play an important role in the minimization of synthesis cost for cells. So, there is a need to maintain a balance between cell performance and the cost concerned with the fabrication process. However, coking and sulfur poisoning can be eliminated by flowing gas between both electrodes [39,40]. A very few studies have been reported highlighting the issues of poisoning behavior of Sulphur redox, carbon deposition, and reversibility towards symmetric electrodes. So, more attention should be devoted to this issue in the future. Symmetric SOFC comprising of two or multiple phases capable to perform various functions could be more promising cells for energy storage devices. By adopting an optimal approach for the selection of materials being used in the fabrication of both electrodes (cathode and anode) overall electrochemical performance of SOFC can be improved. Regardless of all these reported issues, Symmetric electrodes are still falling under the category of high-performance SOFCs cells for various advanced applications and their commercialization in emerging energy fields [120-122].

The selection of the electrode material for the fabrication of SOFCs is another challenging feature as the overall performance of the fuel cell is evaluated by reactions occurring at the anode site. The anode should be of higher electronic conductivity for the evaluation of transported electrons through a channel or reduced resistance. It must be resistant to carburization and sulfide, inert towards electrolytes, and capable of retaining enhanced- catalytic activity. However, the question of low electronic conductivity for the anode in composite electrodes becomes more conventional. Perovskite materials are associated with several cons corresponding to lower electronic conductivity at room temperature and show brittleness under acidic conditions. Hence, their electronic conductivities can be improved by loading a sufficient amount of metals or composites exhibiting higher values of electrical conductance e.g by employing CNT and graphene electrical conductance can be remarkably enhanced. The electronic configuration of perovskite oxides can be tuned for transiting the metal charges to the surface of nanoparticles during spin-state change through the application of the downsizing technique. Low-valence cation doping is considered as one of the promising techniques to transit the structural configuration of metals within the crystal structure due to this reason an increased metal–oxygen covalence and decrease in d-band energy have been observed in several reported studies. In addition, adequate filling of orbitals leads to increased tensile strength that results in enhanced catalytic activity. It is a big challenge for researchers to develop several strategies for controllable and reliable approaches for the production of nanostructured perovskite oxides. Effective industrial implementation of oxygen electrocatalysts in various electro-chemical energy storage and conversion devices is necessary for their proper understanding. For further future advancement in this attractive area, further multidisciplinary approaches including conventional electrochemistry, physics, experimental solid-state chemistry, and advanced characterization with multiscale computing would be important perspectives.

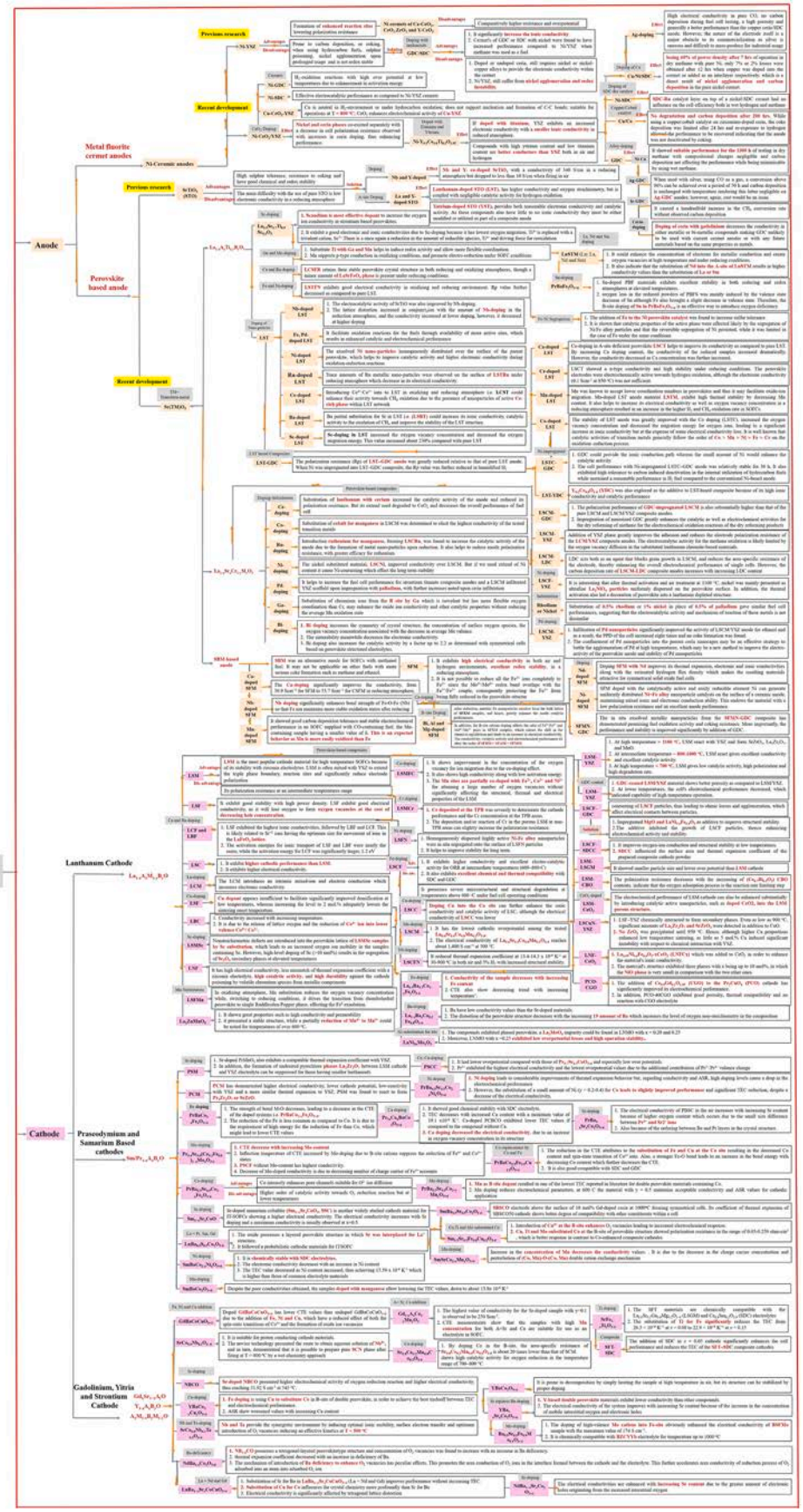

Fig. 9. Summary of Electrode materials for solid oxide fuel cells.

CRediT authorship contribution statement

Muhammad Bilal Hanif: Conceptualization, Methodology, Software, Writing - review & editing, Supervision, Visualization. **Martin Motola:** Validation, Investigation. **Sana qayyum:** Writing - review & editing. **Sajid Rauf:** Validation, Investigation. **Azqa khalid:** Validation, Investigation. **Chang-Jiu Li:** Project administration. **Cheng-Xin Li:** Supervision, Visualization.

Declaration of Competing Interest

The authors declare that they have no known competing financial interests or personal relationships that could have appeared to influence the work reported in this paper.

Acknowledgment

This work was supported by the National Key Research and Development Program of China (Basic Research Project, Grant No. 2017YFB0306100) and the National Key Research and Development Program of China (China-USA Intergovernmental Cooperation Project, Grant NO. 2017YFE0105900) and supported by 111 Project 2.0 (BP0618008).

References

[1] S. Choi, S. Yoo, J. Kim, S. Park, A. Jun, S. Sengodan, G. Kim, Highly efficient and robust cathode materials for low-temperature solid oxide fuel cells: $PrBa_{0.5}Sr_{0.5}Co_{2-x}Fe_xO_{5+\delta}$, Sci. Rep. 3 (2013) 2426.
[2] D.M. Bastidas, S. Tao, J.T. Irvine, A symmetrical solid oxide fuel cell demonstrating redox stable perovskite electrodes, J. Mater. Chem. 16 (2006) 1603–1605.
[3] Q. Liu, X. Dong, G. Xiao, F. Zhao, F. Chen, A novel electrode material for symmetrical SOFCs, Adv. Mater. 22 (2010) 5478–5482.
[4] U. Anjum, M. Agarwal, T.S. Khan, M.A. Haider, Effect of Fe-doping on oxygen anion diffusion in $PrBaCo_{2-x}Fe_xO_{5+\delta}$ double perovskite electrodes for solid oxide fuel cells, ECS Trans. 77 (2017) 125.
[5] Y. Zheng, C. Zhang, R. Ran, R. Cai, Z. Shao, D. Farrusseng, A new symmetric solid-oxide fuel cell with $La_{0.8}Sr_{0.2}Sc_{0.2}Mn_{0.8}O_{3-\delta}$ perovskite oxide as both the anode and cathode, Acta Mater. 57 (2009) 1165–1175.
[6] W. Fan, Z. Sun, J. Zhou, K. Wu, Y. Cheng, Characterization of Sr/Ru co-doped ferrite-based perovskite as a symmetrical electrode material for solid oxide fuel cells, J. Power Sources 348 (2017) 94–106.
[7] Y. Li, Z. Wang, J. Li, X. Zhu, Y. Zhang, X. Huang, Z. Lü, Sulfur poisoning and attempt of oxidative regeneration of $La_{0.75}Sr_{0.25}Cr_{0.5}Mn_{0.5}O_{3-\delta}$ anode for solid oxide fuel cell, J. Alloy. Compd. 698 (2017) 794–799.
[8] A. Hartley, M. Sahibzada, M. Weston, I.S. Metcalfe, D. Mantzavinos, $La_{0.6}Sr_{0.4}Co_{0.2}Fe_{0.8}O_3$ as the symmetrical solid oxide electrolysis temperature solid oxide fuel cells, Catal. Today 55 (2000) 197–204.
[9] H.S. Kim, Y. Jeon, J.H. Kim, G.Y. Jang, S.P. Yoon, J.W. Yun, Characteristics of $Sr_{1-x}Y_xTi_{1-y}Ru_yO_{3+\delta}$ and Ru-impregnated $Sr_{1-x}Y_xTiO_{3+\delta}$ perovskite catalysts as SOFC anode for methane dry reforming, Appl. Surf. Sci. 510 (2020), 145450.
[10] P. Ding, W. Li, H. Zhao, C. Wu, L. Zhao, B. Dong, S. Wang, Review on Ruddlesden-Popper perovskites as cathode for solid oxide fuel cells, Journal of Physics: Materials 4 (2) (2021), 022002.
[11] S.M. Bukhari, J.B. Giorgi, Effect of cobalt substitution on thermal stability and electrical conductivity of $Sm_{0.95}Ce_{0.05}FeO_{3-\delta}$ in oxidizing and reducing conditions, Solid State Ionics 181 (2010) 392–401.
[12] M.Y. Shah, S. Rauf, N. Mushtaq, B. Zhu, Z. Tayyab, M. Yousaf, M.B. Hanif, P. D. Lund, L. Lu, M.I. Asghar, Novel Perovskite Semiconductor Based on Co/Fe-Codoped LBZY ($La_{0.5}Ba_{0.5}Co_{0.2}Fe_{0.2}Zr_{0.3}Y_{0.3}O_{3-\delta}$) as an Electrolyte in Ceramic Fuel Cells, ACS Applied Energy Materials (2021).
[13] L.R. Tarutina, J.G. Lyagaeva, A.S. Farlenkov, A.I. Vylkov, G.K. Vdovin, A. A. Murashkina, D.A. Medvedev, Doped (Nd, Ba) FeO_3 oxides as potential electrodes for symmetrically designed protonic ceramic electrochemical cells, Journal of Solid-State Electrochemistry (2020) 1–10.
[14] P. Niehoff, S. Baumann, F. Schulze-Küppers, R.S. Bradley, I. Shapiro, W. A. Meulenberg, R. Vaßen, Oxygen transport through supported $Ba_{0.5}Sr_{0.5}Co_{0.8}Fe_{0.2}O_{3-\delta}$ membranes, Sep. Purif. Technol. 121 (2014) 60–67.
[15] T. Wei, X. Zhou, Q. Hu, Q. Gao, D. Han, X.S.Wang Lv, A high power density solid oxide fuel cell based on nano-structured $La_{0.8}Sr_{0.2}Cr_{0.5}Fe_{0.5}O_{3-\delta}$ anode, Electrochim. Acta 148 (2014) 33–38.
[16] X. Zhang, S. Ohara, R. Maric, K. Mukai, T. Fukui, H. Yoshida, K. Miura, Ni-SDC cermet anode for medium-temperature solid oxide fuel cell with lanthanum gallate electrolyte, J. Power Sources 83 (1999) 170–177.
[17] A.C.F.M. Costa, M.A.F. Ramalh, L.S. Neiva, L. Gama, S. Alves-Junior, R.H.G. A. Kiminami, Particle size evaluation of the ZnO obtained by the Pechini method, Revista Eletronica de Materiais e Processos 2 (2007) 14–19.
[18] S. Gupta, Y. Zhong, Mahapatra, P. Singh, Processing and electrochemical performance of manganese-doped lanthanum-strontium chromite in oxidizing and reducing atmospheres, Int. J. Hydrogen Energy 40 (2015) 13479–13489.
[19] T. Luo, X. Liu, X. Meng, H. Wu, S. Wang, Z. Zhan, In situ formation of $LaNi_{0.6}Fe_{0.4}O_{3-\delta}$-carbon nanotube hybrids as anodes for direct-methane solid oxide fuel cells, J. Power Sources 299 (2015) 472–479.
[20] X. Liu, D. Han, Y. Zhou, X. Meng, H. Wu, J. Li, Z. Zhan, Sc-substituted $La_{0.6}Sr_{0.4}FeO_{3-\delta}$ mixed conducting oxides as promising electrodes for symmetrical solid oxide fuel cells, J. Power Sources 246 (2014) 457–463.
[21] J.C. Ruiz-Morales, D. Marrero-López, M. Gálvez-Sánchez, J. Canales-Vázquez, C. Savaniu, S.N. Savvin, Engineering of materials for solid oxide fuel cells and other energy and environmental applications, Energy Environ. Sci. 3 (2010) 670–1681.
[22] C. Duan, R.J. Kee, H. Zhu, C. Karakaya, Y. Chen, S. Ricote, R. O'Hayre, Highly durable, coking and sulfur tolerant, fuel-flexible protonic ceramic fuel cells, Nature 557 (2018) 217–222.
[23] J. Canales-Vázquez, J.C. Ruiz-Morales, D. Marrero-López, J. Peña-Martínez, P. Núñez, P. Gómez-Romero, Fe-substituted (La, Sr) TiO_3 as potential electrodes for symmetrical fuel cells (SFCs), J. Power Sources 171 (2007) 552–557.
[24] M. Chen, S. Paulson, V. Thangadurai, V. Birss, Sr-rich chromium ferrites as symmetrical solid oxide fuel cell electrodes, J. Power Sources 236 (2013) 68–79.
[25] A.L. Vincent, J.L. Luo, K.T. Chuang, A.R. Sanger, Promotion of activation of CH_4 by H_2S in oxidation of sour gas over sulfur tolerant SOFC anode catalysts, Appl. Catal. B 106 (2011) 114–122.
[26] A. Vincent, J.L. Luo, K.T. Chuang, A.R. Sange, Effect of Ba doping on performance of LST as anode in solid oxide fuel cells, J. Power Sources 195 (2010) 769–774.
[27] K. Zheng, K. Świerczek, J.M. Polfus, M.F. Sunding, M. Pishahang, T. Norby, Carbon deposition and sulfur poisoning in $SrFe_{0.75}Mo_{0.25}O_{3-\delta}$ and $SrFe_{0.5}Mn_{0.25}Mo_{0.25}O_{3-\delta}$ electrode materials for symmetrical SOFCs, J. Electrochem. Soc. 162 (2015) F1078.
[28] B. He, L. Zhao, S. Song, T. Liu, F. Chen, C. Xia, $Sr_2Fe_{1.5}Mo_{0.5}O_{6-\delta}$-$Sm_{0.2}Ce_{0.8}O_{1.9}$ composite anodes for intermediate-temperature solid oxide fuel cells, J. Electrochem. Soc. 159 (2012) B619.
[29] T. Wei, Q. Zhang, Y.H. Huang, J.B. Goodenough, Cobalt-based double-perovskite symmetrical electrodes with low thermal expansion for solid oxide fuel cells, J. Mater. Chem. 22 (2012) 225–231.
[30] J.C. Ruiz-Morales, J. Canales-Vázquez, J. Peña-Martínez, D.M. López, P. Núñez, On the simultaneous use of $La_{0.75}Sr_{0.25}Cr_{0.5}Mn_{0.5}O_{3-\delta}$ as both anode and cathode material with improved microstructure in solid oxide fuel cells, Electrochim. Acta 52 (2006) 278–284.
[31] S. Tao, J.T. Irvine, Catalytic properties of the perovskite oxide $La_{0.75}Sr_{0.25}Cr_{0.5}Fe_{0.5}O_{3-\delta}$ in relation to its potential as a solid oxide fuel cell anode material, Chem. Mater. 16 (2004) 4116–4121.
[32] Y. Wan, Y. Xing, Z. Xu, S. Xue, S. Zhang, C. Xia, A-site bismuth doping, a new strategy to improve the electrocatalytic performances of lanthanum chromate anodes for solid oxide fuel cells, Appl. Catal. B 269 (2020), 118809.
[33] D.E. Fowler, A.C. Messner, E.C. Miller, B.W. Slone, S.A. Barnett, K. R. Poeppelmeier, Decreasing the polarization resistance of (La, Sr) $CrO_{3-\delta}$ solid oxide fuel cell anodes by combined Fe and Ru substitution, Chem. Mater. 27 (2015) 3683–3693.
[34] P. Boldrin, E. Ruiz-Trejo, J. Mermelstein, J.M. Bermúdez Menéndez, T. Ramírez Reina, N.P. Brandon, Strategies for carbon and sulfur tolerant solid oxide fuel cell materials, incorporating lessons from heterogeneous catalysis, Chem. Rev. 116 (2016) 13633–13684.
[35] W. Xie, M. Fan, Biodiesel production by transesterification using tetraalkylammonium hydroxides immobilized onto SBA-15 as a solid catalyst, Chem. Eng. J. 239 (2014) 60–67.
[36] X. Zhu, Z. Lü, B. Wei, M. Liu, X. Huang, W. Su, A comparison of $La_{0.75}Sr_{0.25}Cr_{0.5}Mn_{0.5}O_{3-\delta}$ and Ni impregnated porous YSZ anodes fabricated in two different ways for SOFCs, Electrochim. Acta 55 (2010) 3932–3938.
[37] M.K. Rath, B.H. Choi, K.T. Lee, Properties and electrochemical performance of $La_{0.75}Sr_{0.25}Cr_{0.5}Mn_{0.5}O_{3-\delta}$-$La_{0.2}Ce_{0.8}O_{2-\delta}$ composite anodes for solid oxide fuel cells, J. Power Sources 213 (2012) 55–62.
[38] J. Karczewski, B. Riegel, M. Gazda, P. Jasinski, B. Kusz, Electrical and structural properties of Nb-doped $SrTiO_3$ ceramics, J. Electroceram. 24 (2010) 26–330.
[39] S. Wang, P.A.W. Van der Heide, C. Chavez, A.J. Jacobson, S.B. Adler, An electrical conductivity relaxation study of $La_{0.6}Sr_{0.4}Fe_{0.8}Co_{0.2}O_{3-\delta}$, Solid State Ionics 156 (2003) 201–208.
[40] H. Kurokawa, L. Yang, C.P. Jacobson, L.C. De Jonghe, S.J. Visco, Y-doped $SrTiO_3$ based sulfur tolerant anode for solid oxide fuel cells, J. Power Sources 164 (2007) 10–518.
[41] M.B. Phillipps, N.M. Sammes, O. Yamamoto, $Gd_{1-x}A_xCo_{1-y}Mn_yO_3$ (A= Sr, Ca) as a cathode for the SOFC, Solid State Ionics 123 (1999) 131–138.
[42] Y. Zhang, H. Zhao, Z. Du, K. Świercze, Y. Li, High-performance $SmBaMn_2O_{5+\delta}$ electrode for symmetrical solid oxide fuel cell, Chem. Mater. 3 (2019) 3784–3793.
[43] G. Yang, C. Su, R. Ran, M.O. Tade, Z. Shao, Advanced symmetric solid oxide fuel cell with an infiltrated K_2NiF_4-type La_2NiO_4 electrode, Energy Fuels 28 (2014) 356–362.
[44] Z. Cao, Y. Zhang, J. Miao, Z. Wang, Z. Lü, Y. Sui, W. Jiang, Titanium-substituted lanthanum strontium ferrite as a novel electrode material for symmetrical solid oxide fuel cell, Int. J. Hydrogen Energy 40 (2015) 16572–16577.
[45] J.S. Yoon, Y.S. Lim, B.H. Choi, H.J. Hwang, Catalytic activity of perovskite-type doped $La_{0.08}Sr_{0.92}Ti_{1-x}M_xO_{3-\delta}$ (M= Mn, Fe, and Co) oxides for methane oxidation, Int. J. Hydrogen Energy 39 (2014) 7955–7962.

[46] B. Iwanschitz, L. Holzer, A. Mai, M. Schütze, Nickel agglomeration in solid oxide fuel cells: The influence of temperature, Solid State Ionics 211 (2012) 69–73.

[47] B.H. Park, G.M. Choi, Ex-solution of Ni nanoparticles in a $La_{0.2}Sr_{0.8}Ti_{1-x}Ni_xO_{3-\delta}$ alternative anode for solid oxide fuel cell, Solid State Ionics 262 (2014) 345–348.

[48] B.H. Park, G.M. Choi, Effect of anode firing on the performance of lanthanum and nickel co-doped $SrTiO_3$ ($La_{0.2}Sr_{0.8}Ti_{0.9}Ni_{0.1}O_{3-\delta}$) anode of solid oxide fuel cell, J. Power Sources 293 (2015) 684–691.

[49] D. Neagu, G. Tsekouras, D.N. Miller, H. Ménard, J.T. Irvine, In situ growth of nanoparticles through control of non-stoichiometry, Nat. Chem. 5 (2013) 916–923.

[50] S. Sengodan, S. Choi, A. Jun, T.H. Shin, Y.W. Ju, H.Y. Jeong, G. Kim, Layered oxygen-deficient double perovskite as an efficient and stable anode for direct hydrocarbon solid oxide fuel cells, Nat. Mater. 14 (2015) 205–209.

[51] Z. Du, H. Zhao, S. Yi, Q. Xia, Y. Gong, Y. Zhang, K. Świerczek, High-performance anode material $Sr_2FeMo_{0.65}Ni_{0.35}O_{6-\delta}$ with in situ exsolved nanoparticle catalyst, ACS Nano 10 (2016) 8660–8669.

[52] O. Kwon, K. Kim, S. Joo, H.Y. Jeong, J. Shin, J.W. Han, G. Kim, Self-assembled alloy nanoparticles in a layered double perovskite as a fuel oxidation catalyst for solid oxide fuel cells, J. Mater. Chem. A 6 (2018) 15947–15953.

[53] T.M. Gür, Comprehensive review of methane conversion in solid oxide fuel cells: prospects for efficient electricity generation from natural gas, Prog. Energy Combust. Sci. 54 (2016) 1–64.

[54] K. Zheng, K. Świerczek, Physicochemical properties of rock salt-type ordered Sr_2MMoO_6 (M= Mg, Mn, Fe Co, Ni) double perovskites, J. Eur. Ceram. Soc. 34 (2014) 4273–4284.

[55] Y.H. Huang, G. Liang, M. Croft, M. Lehtimaki, M. Karppinen, J.B. Goodenough, Double-perovskite anode materials Sr_2MMoO_6 (M= Co, Ni) for solid oxide fuel cells, Chem. Mater. 21 (2009) 2319–2326.

[56] F.Y. Wang, G.B. Zhong, S. Luo, L. Xia, L.H. Fang, X. Song, G. Yan, Porous $Sr_2MgMo_{1-x}V_xO_{6-\delta}$ ceramics as anode materials for SOFCs using biogas fuel, Catal. Commun. 67 (2015) 108–111.

[57] D. Neagu, V. Kyriakou, I.L. Roiban, M. Aouine, C. Tang, A. Caravaca, M. N. Tsampas, In situ observation of nanoparticle exsolution from perovskite oxides: from atomic scale mechanistic insight to nanostructure tailoring, ACS Nano 13 (2019) 12996–13005.

[58] Y. Liu, S. Wang, J. Qian, X. Xin, Z. Zhan, T. Wen, A novel catalytic layer material for direct dry methane solid oxide fuel cell, Int. J. Hydrogen Energy 38 (2013) 14053–14059.

[59] P.I. Cowin, R. Lan, C.T. Petit, S. Tao, Conductivity and redox stability of perovskite oxide $SrFe_{1-x}Ti_xO_{3-\delta}$ ($x \leq 0.3$), Solid State Sci. 46 (2015) 62–70.

[60] R. Lan, P.I. Cowin, S. Sengodan, S. Tao, A perovskite oxide with high conductivities in both air and reducing atmosphere for use as electrode for solid oxide fuel cells, Sci. Rep. 6 (2016) 1–8.

[61] F. Liu, L. Zhang, G. Huang, B. Niu, X. Li, L. Wang, Y. Jin, High performance ferrite–based anode $La_{0.5}Sr_{0.5}Fe_{0.9}Mo_{0.1}O_{3-\delta}$ for intermediate–temperature solid oxide fuel cell, Electrochim. Acta 255 (2017) 118–126.

[62] H. Choi, A. Fuller, D. Dogu, K.E. Binkley, J. Davis, U.S. Ozkan, Effect of Ce doping on the performance and stability of strontium cobalt ferrite perovskites as SOFC anode catalysts, Top. Catal. 58 (2015) 359–374.

[63] X. Wu, X. Zhou, Y. Tian, X. Kong, J. Zhang, W. Zuo, X. Ye, Stability and electrochemical performance of lanthanum ferrite-based composite SOFC anodes in hydrogen and carbon monoxide, Electrochim. Acta 208 (2016) 164–173.

[64] L. Fan, T. Cong, X. Su, Q. Hu, Y. Wang, X. Liu, Y. Xiong, Evaluation of sulfur poisoning and carbon deposition on Co-infiltrated SOFCs $La_{0.4}Sr_{0.6}TiO_3$-$Gd_{0.2}Ce_{0.8}O_{1.9}$ Composite Anodes, Int. J. Electrochem. Sci 15 (2020) 2839–2850.

[65] Z. Du, H. Zhao, X. Zhou, Z. Xie, C. Zhang, Electrical conductivity and cell performance of $La_{0.3}Sr_{0.7}Ti_{1-x}Cr_xO_{3-\delta}$ perovskite oxides used as anode and interconnect material for SOFCs, Int. J. Hydrogen Energy 38 (2013) 1068–1073.

[66] M.K. Rath, B.G. Ahn, B.H. Choi, M.J. Ji, K.T. Lee, Effects of manganese substitution at the B-site of lanthanum-rich strontium titanate anodes on fuel cell performance and catalytic activity, Ceram. Int. 39 (2013) 6343–6353.

[67] K. Shaheen, H. Suo, Z. Shah, M.B. Hanif, Z. Hussain, S. Ali, Y. Wang, Electrochemical performance of multifuel based nanocomposite for Solid Oxide Fuel Cell, Ceram. Int. 46 (2020) 8832–8838.

[68] X. Yang, J. Chen, D. Panthi, B. Niu, L. Lei, Z. Yuan, T. He, Electron doping of $Sr_2FeMoO_{6-\delta}$ as high-performance anode materials for solid oxide fuel cells, J. Mater. Chem. A 7 (2019) 733–743.

[69] C. Bernuy-Lopez, L. Rioja-Monllor, T. Nakamura, S. Ricote, R. O'Hayre, K. Amezawa, T. Grande, Effect of cation ordering on the performance and chemical stability of layered double perovskite cathodes, Materials 11 (2) (2018) 196.

[70] Y. Liu, Y. Tang, Z. Ma, M. Singh, Y. He, W. Dong, B. Zhu, Flower like CeO_2 microspheres coated with $Sr_2Fe_{1.5}Mo_{0.5}O_x$ nanoparticles for an advanced fuel cell, Sci. Rep. 5 (2015) 1–9.

[71] Y. Wang, P. Li, H. Li, Y. Zhao, Y. Li, Synthesis and Enhanced Electrochemical Performance of Sm-Doped $Sr_2Fe_{1.5}Mo_{0.5}O_6$, Fuel Cells 14 (2014) 973–978.

[72] D.A. Osinkin, E.P. Antonova, K.S. Shubin, N.M. Bogdanovich, Influence of nickel exsolution on the electrochemical performance and rate-determining stages of hydrogen oxidation on $Sr_{1.95}Fe_{1.4}Ni_{0.1}Mo_{0.5}O_{6-\delta}$ promising electrode for solid state electrochemical devices, Electrochim. Acta 369 (2021), 137673.

[73] A. Masuno, M. Haruta, M. Azuma, H. Kurata, S. Isoda, M. Takano, Y. Shimakawa, Epitaxial growth and B-site cation ordering in layered double perovskite La_2CuSnO_6 thin films, Appl. Phys. Lett. 89 (21) (2006), 211913.

[74] M. Chen, S. Bao, Y. Zhang, Y. Wang, Y. Liang, J. Wu, C. Chen, Physical and chemical strains co-tuned magnetic properties of double perovskite $PrBaMn_2O_{5+\delta}$ epitaxial films, Appl. Phys. Lett. 115 (2019), 081903.

[75] A. Olafsen, H. Fjellvåg, B.C. Hauback, Crystal Structure and Properties of $Nd_4Co_3O_{10+\delta}$ and $Nd_4Ni_3O_{10-\delta}$, J. Solid State Chem. 151 (2000) 46–55.

[76] J. Shen, G. Yang, Z. Zhang, M.O. Tadé, W. Zhou, Z. Shao, Improved performance of a symmetrical solid oxide fuel cell by swapping the roles of doped ceria and $La_{0.6}Sr_{1.4}MnO_{4+\delta}$ in the electrode, J. Power Sources 342 (2017) 644–651.

[77] A.M. Andringa, A. Perrotta, K. de Peuter, H.C. Knoops, W.M. Kessels, M. Creatore, Low-temperature plasma-assisted atomic layer deposition of silicon nitride moisture permeation barrier layers, ACS Appl. Mater. Interfaces 7 (40) (2015) 22525–22532.

[78] E.P. Murray, M.J. Sever, S.A. Barnett, Electrochemical performance of (La, Sr)(Co, Fe)O_3-(Ce, Gd) O_3 composite cathodes, Solid State Ionics 148 (2002) 27–34.

[79] K. Chen, N. Li, N. Ai, Y. Cheng, W.D. Rickard, S.P. Jiang, Polarization-induced interface and Sr segregation of in situ assembled $La_{0.6}Sr_{0.4}Co_{0.2}Fe_{0.8}O_{3-\delta}$ electrodes on Y_2O_3-ZrO_2 electrolyte of solid oxide fuel cells, ACS applied materials & interfaces 8 (2016) 31729–31737.

[80] K. Develos-Bagarinao, H. Yokokawa, H. Kishimoto, T. Ishiyama, K. Yamaji, T. Horita, Elucidating the origin of oxide ion blocking effects at GDC/SrZr (Y) O_3/YSZ interfaces, J. Mater. Chem. A 5 (2017) 8733–8743.

[81] L. Kindermann, D. Das, H. Nickel, K. Hilpert, Chemical compatibility of the $LaFeO_3$ base perovskites $(La_{0.6}Sr_{0.4})_zFe_{0.8}M_{0.2}O_{3-\delta}$ (z= 1, 0.9; M= Cr, Mn Co, Ni) with yttria stabilized zirconia, Solid State Ionics 89 (1996) 215–220.

[82] L. Miao, J. Hou, Z. Gong, Z. Jin, W. Liu, A high-performance cobalt-free Ruddlesden-Popper phase cathode $La_{1.2}Sr_{0.8}Ni_{0.6}Fe_{0.4}O_{4+\delta}$ for low temperature proton-conducting solid oxide fuel cells, Int. J. Hydrogen Energy 44 (2019) 7531–7537.

[83] R. Li, F. Jin, Y. Zhang, B. Niu, J. Liu, T. He, Performance and optimization of perovskite-type $La_{1.4}Ca_{0.6}CoMnO_{5+\delta}$ cathode for intermediate-temperature solid oxide fuel cells, Int. J. Hydrogen Energy 44 (2019) 8467–8478.

[84] S. Le, C. Li, X. Song, Y. Zhang, Y. Feng, Y. Mao, Z. Yuan, A novel Nb and Cu co-doped $SrCoO_{3-\delta}$ cathode for intermediate temperature solid oxide fuel cells, Int. J. Hydrogen Energy 45 (18) (2020) 10862–10870.

[85] C. Duan, D. Hook, Y. Chen, J. Tong, R. O'Hayre, Zr and Y co-doped perovskite as a stable, high performance cathode for solid oxide fuel cells operating below 500 °C, Energy Environ. Sci. 10 (2017) 176–182.

[86] C. Xia, Y. Mi, B. Wang, B. Lin, G. Chen, B. Zhu, Shaping triple-conducting semiconductor $BaCo_{0.4}Fe_{0.4}Zr_{0.1}Y_{0.1}O_{3-\delta}$ into an electrolyte for low-temperature solid oxide fuel cells, Nat. Commun. 10 (2019) 1–9.

[87] I.M. Hung, J.A. Wang, J.Y. Kuo, T.N. Lin, Material Characteristics and Electrochemical Performance of $Y_xBa_{2-X}Co_2O_{5+\delta}$ Cathode for Solid Oxide Fuel Cell, ECS Trans. 68 (1) (2015) 919.

[88] F. Lu, T. Xia, Q. Li, J. Wang, L. Huo, H. Zhao, Heterostructured simple perovskite nanorod-decorated double perovskite cathode for solid oxide fuel cells: Highly catalytic activity, stability and CO_2-durability for oxygen reduction reaction, Appl. Catal. B 249 (2019) 19–31.

[89] U. Anjum, M. Agarwal, T.S. Khan, M.A. Haider, Ca-doped double perovskite $PrBa_{0.8}Ca_{0.2}Co_2O_{5+\delta}$ thin-film electrodes: Experimental and theoretical study, ECS Trans. 78 (2017) 499.

[90] C. Lim, A. Jun, H. Jo, K.M. Ok, J. Shin, Y.W. Ju, G. Kim, Influence of Ca-doping in layered perovskite $PrBaCo_2O_{5+\delta}$ on the phase transition and cathodic performance of a solid oxide fuel cell, J. Mater. Chem. A 4 (2016) 6479–6486.

[91] S. Afroze, A. Karim, Q. Cheok, S. Eriksson, A.K. Azad, Latest development of double perovskite electrode materials for solid oxide fuel cells: a review, Frontiers in Energy 13 (4) (2019) 770–797.

[92] W. Mao, Q. Yao, Y. Fan, Y. Wang, X. Wang, Y. Pu, X.A. Li, Combined experimental and theoretical investigation on modulation of multiferroic properties in $BiFeO_3$ ceramics induced by Dy and transition metals co-doping, J. Alloy. Compd. 784 (2019) 117–124.

[93] M.N. Sithole, B. Omondi, P.G. Ndungu, Synthesis and characterization of $Ce_{0.6}Sr_{0.4}Fe_{0.8}Co_{0.2}O_{3-\delta}$ perovskite material: Potential cathode material for low temperature SOFCs, J. Rare Earths 35 (2017) 389–397.

[94] H. Liu, K. Zhu, Y. Liu, W. Li, L. Cai, X. Zhu, W. Yang, Structure and electrochemical properties of cobalt-free perovskite cathode materials for intermediate-temperature solid oxide fuel cells, Electrochim. Acta 279 (2018) 224–230.

[95] S. Yoo, J.Y. Shin, G. Kim, Thermodynamic and electrical characteristics of $NdBaCo_2O_{5+\delta}$ at various oxidation and reduction states, J. Mater. Chem. 21 (2011) 439–443.

[96] L. Zhao, J. Shen, B. He, F. Chen, C. Xia, Synthesis, characterization and evaluation of $PrBaCo_{2-x}Fe_xO_{5+\delta}$ as cathodes for intermediate-temperature solid oxide fuel cells, Int. J. Hydrogen Energy 36 (2011) 3658–3665.

[97] S. Duran, J. Tellez, M.V. Sandoval, M.A. Macias, E. Capoen, C. Pirovano, G. H. Gauthier, Study of $La_4BaCu_{5-x}Co_xO_{13+\delta}$ series as potential cathode materials for intermediate-temperature solid oxide fuel cell, Solid State Ionics 326 (2018) 116–123.

[98] M. Saccoccio, C. Jiang, Y. Gao, D. Chen, F. Ciucci, Nb-substituted $PrBaCo_2O_{5+\delta}$ as a cathode for solid oxide fuel cells: a systematic study of structural, electrical, and electrochemical properties, Int. J. Hydrogen Energy 42 (2017) 19204–19215.

[99] B. Wang, G. Long, Y. Li, H. Jia, D. Qiu, J. Wang, Y. Ji, Synthesis and characterization of $Ba0.5Sr0.5Co0.8Fe0.1Ni0.1O_{3-\delta}$ cathode for intermediate-temperature solid oxide fuel cells, Int. J. Hydrogen Energy 43 (2018) 6677–6685.

[100] J.H. Kim, M. Cassidy, J.T. Irvine, J. Bae, Advanced electrochemical properties of $LnBa_{0.5}Sr_{0.5}Co_2O_{5+\delta}$ (Ln= Pr, Sm, and Gd) as cathode materials for IT-SOFC, J. Electrochem. Soc. 156 (2009) B682.

[101] M. Zhu, Z. Cai, T. Xia, Q. Li, L. Huo, H. Zhao, Cobalt-free perovskite $BaFe_{0.85}Cu_{0.15}O_{3-\delta}$ cathode material for intermediate-temperature solid oxide fuel cells, Int. J. Hydrogen Energy 41 (2016) 4784–4791.

[102] F. Dong, Y. Chen, R. Ran, D. Chen, M.O. Tadé, S. Liu, Z. Shao, $BaNb_{0.05}Fe_{0.95}O_{3-\delta}$ as a new oxygen reduction electrocatalyst for intermediate temperature solid oxide fuel cells, J. Mater. Chem. A 1 (2013) 9781–9791.

[103] K. Shaheen, Z. Shah, H. Gulab, M.B. Hanif, H. Suo, Metal oxide nanocomposites as anode and cathode for low temperature solid oxide fuel cell, Solid State Sci. 102 (2020), 106162.

[104] M.B. Hanif, J.T. Gao, K. Shaheen, Y.P. Wang, M. Yasir, S.L. Zhang, C.X. Li, Performance evaluation of highly active and novel $La_{0.7}Sr_{0.3}Ti_{0.1}Fe_{0.6}Ni_{0.3}O_{3-\delta}$ material both as cathode and anode for intermediate-temperature symmetrical solid oxide fuel cell, J. Power Sources 472 (2020), 228498.

[105] Q. Zhou, C. Yuan, D. Han, T. Luo, J. Li, Z. Zhan, Evaluation of $LaSr_2Fe_2CrO_{9-\delta}$ as a potential electrode for symmetrical solid oxide fuel cells, Electrochim. Acta 133 (2014) 453–458.

[106] J. Zhou, G. Chen, K. Wu, Y. Cheng, The performance of $La_{0.6}Sr_{1.4}MnO_4$ layered perovskite electrode material for intermediate temperature symmetrical solid oxide fuel cells, J. Power Sources 270 (2014) 418–425.

[107] R. Martınez-Coronado, A. Aguadero, D. Pérez-Coll, L. Troncoso, J.A. Alonso, M. T. Fernández-Dıaz, Characterization of $La_{0.5}Sr_{0.5}Co_{0.5}Ti_{0.5}O_{3-\delta}$ as symmetrical electrode material for intermediate-temperature solid-oxide fuel cells, Int. J. Hydrogen Energy 37 (2012) 1831.

[108] B. He, C. Gong, Z. Wang, L. Jia, L. Zhao, Novel, cobalt-free, and highly active $Sr_2Fe_{1.5}Mo_{0.5-x}Sn_xO_{6-\delta}$ cathode materials for intermediate temperature solid oxide fuel cells, Int. J. Hydrogen Energy 42 (2017) 10308–10316.

[109] F. Liang, Z. Wang, Z. Wang, J. Mao, J. Sunarso, Electrochemical Performance of Cobalt-Free Nb and Ta Co-Doped Perovskite Cathodes for Intermediate-Temperature Solid Oxide Fuel Cells, ChemElectroChem 4 (2017) 2366–2372.

[110] M. Li, W. Zhou, X. Xu, Z. Zhu, $SrCo_{0.85}Fe_{0.1}P_{0.05}O_{3-\delta}$ perovskite as a cathode for intermediate-temperature solid oxide fuel cells, J. Mater. Chem. A 1 (2013) 13632–13639.

[111] W. Zhou, W. Jin, Z. Zhu, Z. Shao, Structural, electrical and electrochemical characterizations of $SrNb_{0.1}Co_{0.9}O_{3-\delta}$ as a cathode of solid oxide fuel cells operating below 600 °C, Int. J. Hydrogen Energy 35 (2010) 1356–1366.

[112] A.K. Tomar, G. Singh, R.K. Sharma, Fabrication of a Mo-doped strontium cobaltite perovskite hybrid supercapacitor cell with high energy density and excellent cycling life, Chem Sus Chem 11 (2018) 4123–4130.

[113] V. Cascos, R. Martínez-Coronado, J.A. Alonso, New Nb-doped $SrCo_{1-x}Nb_xO_{3-\delta}$ perovskites performing as cathodes in solid-oxide fuel cells, Int. J. Hydrogen Energy 39 (2014) 14349–14354.

[114] Y. Zhu, J. Sunarso, W. Zhou, S. Jiang, Z. Shao, High-performance $SrNb_{0.1}Co_{0.9-x}Fe_xO_{3-\delta}$ perovskite cathodes for low-temperature solid oxide fuel cells, J. Mater. Chem. A 2 (2014) 15454–15462.

[115] A.U. Rehman, Development of CO_2 tolerant cathode materials for low-temperature solid oxide fuel, cells (2020).

[116] G. Chen, Y. Wang, J. Sunarso, F. Liang, H. Wang, A new scandium and niobium co-doped cobalt-free perovskite cathode for intermediate-temperature solid oxide fuel cells, Energy 95 (2016) 137–143.

[117] Z. Yang, G. Xia, J.W. Stevenson, $Mn_{1.5}Co_{1.5}O_4$ spinel protection layers on ferritic stainless steels for SOFC interconnect applications, Electrochem. Solid-State Lett. 8 (2005) A168.

[118] M. Li, W. Zhou, V.K. Peterson, M. Zhao, Z. Zhu, A comparative study of $SrCo_{0.8}Nb_{0.2}O_{3-\delta}$ and $SrCo_{0.8}Ta_{0.2}O_{3-\delta}$ as low-temperature solid oxide fuel cell cathodes: effect of non-geometry factors on the oxygen reduction reaction, J. Mater. Chem. A 3 (2015) 24064–24070.

[119] M.F.R. Samsudin, H. Ullah, A.A. Tahir, X. Li, Y.H. Ng, S. Sufian, Superior photoelectrocatalytic performance of ternary structural $BiVO_4$/GQD/g-C_3N_4 heterojunction, J. Colloid Interface Sci. 586 (2021) 785–796.

[120] Y. Cao, Z. Zhu, Y. Zhao, W. Zhao, Z. Wei, T. Liu, Development of tungsten stabilized $SrFe_{0.8}W_{0.2}O_{3-\delta}$ material as novel symmetrical electrode for solid oxide fuel cells, J. Power Sources 455 (2020), 227951.

[121] B. Niu, F. Jin, L. Zhang, P. Shen, T. He, Performance of double perovskite symmetrical electrode materials $Sr_2TiFe_{1-x}Mo_xO_{6-\delta}$ (x= 0.1, 0.2) for solid oxide fuel cells, Electrochim. Acta 263 (2018) 217–227.

[122] X. Lu, Y. Yang, Y. Ding, Y. Chen, Q. Gu, D. Tian, B. Lin, Mo-doped $Pr_{0.6}Sr_{0.4}Fe_{0.8}Ni_{0.2}O_{3-\delta}$ as potential electrodes for intermediate-temperature symmetrical solid oxide fuel cells, Electrochim. Acta 227 (2017) 33–40.

[123] Y. Wu, Y. Yang, S. Zhou, W. Zhu, W. Song, H. Bao, Y. Ling, Enhanced redox-stable $Sm_{0.5}Sr_{0.5}FeO_{3-\delta}$ electrode material for symmetric solid oxide fuel cells at reduced temperatures, Ceram. Int. 46 (2020) 6714–6722.

[124] Y. Yu, L. Yu, K. Shao, Y. Li, K. Maliutina, W. Yuan, L. Fan, $BaZr_{0.1}Co_{0.4}Fe_{0.4}Y_{0.1}O_3$-SDC composite as quasi-symmetrical electrode for proton conducting solid oxide fuel cells, Ceram. Int. 46 (2020) 11811–11818.

[125] B. An, W. Zhou, Y. Guo, R. Ran, Z. Shao, A composite oxygen-reduction electrode composed of $SrSc_{0.2}Co_{0.8}O_{3-\delta}$ perovskite and $Sm_{0.2}Ce_{0.8}O_{1.9}$ for an intermediate-temperature solid-oxide fuel cell, Int. J. Hydrogen Energy 35 (2010) 5601–5610.

[126] L. Da-Conceição, C.R. Silva, N.F. Ribeiro, M.M. Souza, Influence of the synthesis method on the porosity, microstructure and electrical properties of $La_{0.7}Sr_{0.3}MnO_3$ cathode materials, Mater. Charact. 60 (2009) 1417–1423.

[127] P. Matheswaran, M. Rajasekhar, A. Subramania, Assisted combustion synthesis and characterization of $Pr_{0.6}Sr_{0.4}MnO_{3\pm\delta}$ nano crystalline powder as cathode material for IT-SOFC, Ceram. Int. 43 (2017) 988–991.

[128] M. Tatko, M. Mosiałek, M. Dudek, P. Nowak, A. Kędra, E. Bielańska, Composite cathode materials $Sm_{0.5}Sr_{0.5}CoO_3$-$La_{0.6}Sr_{0.4}FeO_3$ for solid oxide fuel cells, Solid State Ionics 271 (2015) 103–108.

[129] W. Li, J. Pu, B. Chi, L. Jian, $Sm_{0.5}Sr_{0.5}MnO_3$ as a potential cathode material for intermediate temperature solid oxide fuel cells, Electrochim. Acta 141 (2014) 189–194.

[130] Y. Tian, W. Wang, Y. Liu, L. Zhang, L. Jia, J. Yang, J. Li, Cobalt-Free Perovskite Oxide $La_{0.6}Sr_{0.4}Fe_{0.8}Ni_{0.2}O_{3-\delta}$ as Active and Robust Oxygen Electrode for Reversible Solid Oxide Cells, ACS Applied Energy Materials 2 (2019) 3297–3305.

[131] I.M. Hung, J.S. Wu, Y.W. Hsu, Y.C. Lee, Effect of Morphology of $La_{0.8}Sr_{0.2}Co_{0.2}Fe_{0.8}O_{3-\delta}$ Cathode on the Electrochemical Performance of Solid Oxide Fuel Cell, J. Chin. Chem. Soc. 59 (2012) 1329–1336.

[132] Y. Zhang, J. Liu, X. Huang, Z. Lu, W. Su, Low temperature solid oxide fuel cell with $Ba_{0.5}Sr_{0.5}Co_{0.8}Fe_{0.2}O_3$ cathode prepared by screen printing, Solid State Ionics 179 (2008) 250–255.

[133] Y. Song, Y. Chen, M. Xu, W. Wang, Y. Zhang, G. Yang, Z. Shao, A Cobalt-Free Multi-Phase Nanocomposite as Near-Ideal Cathode of Intermediate-Temperature Solid Oxide Fuel Cells Developed by Smart Self-Assembly, Adv. Mater. 32 (2020) 1906979.

[134] Y. Xia, Y. Teng, H. Lv, Z. Jin, D. Wang, R. Peng, W. Liu, A novel $BaFe_{0.8}Zn_{0.1}Bi_{0.1}O_{3-\delta}$ cathode for proton conducting solid oxide fuel cells, Ceram. Int. 46 (2020) 25453–25459.

[135] H. Jiang, F. Zhang, A Novel Cobalt-free $La_{0.6}Sr_{0.4}Fe_{0.9}Nb_{0.1}O_3$ Cathode for Medium Temperature Solid Oxide Fuel Cells, Int. J. Electrochem. Sci. 15 (2020) 959–965.

[136] H. Li, B. Wei, C. Su, C. Wang, Z. Lü, Novel cobalt-free layered perovskite $LaBaFe_{2-x}Nb_xO_{6-\delta}$ (x= 0–0.1) as cathode for solid oxide fuel cells, J. Power Sources 453 (2020), 227875.

[137] H. Li, Z. Lü, A highly stable cobalt-free $LaBa_{0.5}Sr_{0.5}Fe_2O_{6-\delta}$ oxide as a high-performance cathode material for solid oxide fuel cells, Int. J. Hydrogen Energy 45 (2020) 19831–19839.

[138] Z. Wang, P. Lv, L. Yang, R. Guan, J. Jiang, F. Jin, T. He, $Ba_{0.95}La_{0.05}Fe_{0.8}Zn_{0.2}O_{3-\delta}$ cobalt-free perovskite as a triple-conducting cathode for proton-conducting solid oxide fuel cells, Ceram. Int. 46 (2020) 18216–18223.

[139] F. Zhang, Z. Yang, H. Wang, W. Wang, G. Ma, Performance of Cobalt-free $La_{0.6}Sr_{0.4}Fe_{0.9}Ni_{0.1}O_{3-\delta}$ Cathode Material for Intermediate Temperature Solid Oxide Fuel Cells, Fuel Cells 12 (2012) 749–753.

[140] B. Lin, H. Ding, Y. Dong, S. Wang, X. Zhang, D. Fang, G. Meng, Intermediate-to-low temperature protonic ceramic membrane fuel cells with $Ba_{0.5}Sr_{0.5}Co_{0.8}Fe_{0.2}O_{3-\delta}$-$BaZr_{0.1}Ce_{0.7}Y_{0.2}O_{3-\delta}$ composite cathode, J. Power Sources 186 (2009) 58–61.

[141] Y. Huang, J. Ding, Y. Xia, L. Miao, K. Li, Q. Zhang, W. Liu, $Ba_{0.5}Sr_{0.5}Co_{0.8-x}Fe_{0.2}Nb_xO_{3-\delta}$ (x≤ 0.1) as cathode materials for intermediate temperature solid oxide fuel cells with an electron-blocking interlayer, Ceram. Int. 46 (2020) 10215–10223.

[142] W. Xia, Q. Li, L. Sun, L. Huo, H. Zhao, Enhanced electrochemical performance and CO_2 tolerance of $Ba_{0.95}La_{0.05}Fe_{0.85}Cu_{0.15}O_{3-\delta}$ as Fe-based cathode electrocatalyst for solid oxide fuel cells, J. Eur. Ceram. Soc. 40 (2020) 1967–1974.

[143] Q. Zhou, L. Xu, Y. Guo, D. Jia, Y. Li, W.C.J. Wei, $La_{0.6}Sr_{0.4}Fe_{0.8}Cu_{0.2}O_{3-\delta}$ perovskite oxide as cathode for IT-SOFC, Int. J. Hydrogen Energy 37 (2012) 11963–11968.

[144] A. Idrees, X. Jiang, G. Liu, H. Luo, G. Jia, Q. Zhang, B. Xu, Structures and Properties of $LaFe_{0.8}Cu_{0.2}O_{3-\delta}$ and $BaFe_{0.8}Cu_{0.2}O_{3-\delta}$ as Cobalt-Free Perovskite-Type Cathode Materials for the Oxygen Reduction Reaction, Chemistry Open 7 (2018) 688–695.

[145] C. Sun, Y. Kong, L. Shao, K. Sun, N. Zhang, Probing oxygen vacancy effect on oxygen reduction reaction of the $NdBaCo_2O_{5+\delta}$ cathode for solid oxide fuel cells, J. Power Sources 459 (2020), 228017.

[146] K. Zheng, Ti-doped $Sr_2Fe_{1.4-x}Ti_xMo0_6O_{6-\delta}$ double perovskites with improved stability as anode materials for Solid Oxide Fuel Cells, Mater. Res. Bull. (2020), 110877.

[147] M. Li, M. Zhao, F. Li, W. Zhou, V.K. Peterson, X. Xu, Z. Zhu, A niobium and tantalum co-doped perovskite cathode for solid oxide fuel cells operating below 500 °C, Nat. Commun. 8 (2017) 1–9.

[148] H. Ding, Z. Tao, S. Liu, J. Zhang, A high-performing sulfur-tolerant and redox-stable layered perovskite anode for direct hydrocarbon solid oxide fuel cells, Sci. Rep. 5 (2015) 1–9.

[149] Q. Liu, C. Yang, X. Dong, F. Chen, Perovskite $Sr_2Fe_{1.5}Mo_{0.5}O_{6-\delta}$ as electrode materials for symmetrical solid oxide electrolysis cells, Int. J. Hydrogen Energy 35 (2010) 10039–10044.

[150] Z. Zhang, D. Chen, J. Wang, S. Tan, X. Yu, Z. Shao, Highly active and stable cobalt-free hafnium-doped $SrFe_{0.9}Hf_{0.1}O_{3-\delta}$ perovskite cathode for solid oxide fuel cells, ACS Applied Energy Materials 1 (2018) 2134–2142.

[151] Z. Yang, N. Xu, M. Han, F. Chen, Performance evaluation of $La_{0.4}Sr_{0.6}Co_{0.2}Fe_{0.7}Nb_{0.1}O_{3-\delta}$ as both anode and cathode material in solid oxide fuel cells, Int. J. Hydrogen Energy 39 (2014) 7402–7406.

[152] M.B. Hanif, J.T. Gao, K. Shaheen, Y.P. Wang, M. Yasir, C.J. Li, C.X. Li, Highly active and novel Asite deficient symmetric electrode material $(Sr_{0.3}La_{0.7})_{1-x}(Fe_{0.7}Ti_{0.3})_{0.9}Ni_{0.1}O_{3-\delta}$ and its effect on electrochemical performance of SOFCs, Int. J. Hydrogen Energy 46 (2021) 8778–8791.

[153] M.B. Hanif, J.T. Gao, K. Shaheen, Y.P. Wang, M. Yasir, C.J. Li, C.X. Li, Microstructural analysis of highly active cathode material $La_{0.7}Sr_{0.3}Ti_{0.15}Fe_{0.65}Ni_{0.2}O_{3-\delta}$ (LSTFN) by optimizing different processing parameters, Ceram. Int. 47 (2021) 10893–10904.

[154] H. Yang, M.B. Hanif, S.L. Zhang, C.J. Li, C.X. Li, Sintering behavior and electrochemical performance of A-site deficient $Sr_xTi_{0.3}Fe_{0.7}O_{3-\delta}$ oxygen electrodes for solid oxide electrochemical cells, Ceram. Int. (2021).

[155] M. Burriel, M. Casas-Cabanas, J. Zapata, H. Tan, J. Verbeeck, C. Solis, J. Santiso, Influence of the microstructure on the high-temperature transport properties of $GdBaCo_2O_{5.5+\delta}$ epitaxial films, Chem. Mater. 22 (2019) 5512–5520.

[156] Z. Zhang, B.J. Kennedy, C.J. Howard, L.Y. Jang, K.S. Knight, M. Matsuda, M. Miyake, X-ray absorption and neutron diffraction studies of $(Sr_{1-x}Ce_x)MnO_3$:

transition from coherent to incoherent static Jahn-Teller distortions, J. Phys.: Condens. Matter 22 (2010), 445401.

Muhammad Bilal Hanif has joined Xi'an Jiaotong University (XJTU), China for his MS under a Chinese government scholarship. Now He is working as a research scholar at XJTU with a collaborative projects of Prof. Dr. Cheng-Xin Li. His research mainly focuses on solid oxide fuel cells, super capacitors, and solid oxide electrolysis cells for energy conversion. He has published well renowned international journal papers on energy storage applications.

Professor Dr. Cheng-Xin Li obtained his Ph.D. degree in Materials Science & Engineering at Xi'an Jiao-tong University, China in 2005. He became a professor at Xian Jiao-tong University in 2012, where he leads a research group focused on Solid Oxide Fuel Cells (Materials, Single Cells, Stack, and System). He has worked as a visiting scholar in the University of Technology of Belfort-Montbéliard, Belfort, France in 2015 and Georgia Institute of Technology, Atlanta, the USA from 2017-2019. He has 350 SCI papers publications in international academic journals and more than 50 invention patents with 10,000 citations.

Prof. Dr. Chang-Jiu Li completed his Masters and Doctoral degree in 1986 and 1989 respectively from Osaka University, Japan. He has expertise in diverse fields of research including mechanisms of thermal spray coatings, the coating structure and property characterization, application of thermal spraying technology, and Solid Oxide Fuel Cells. He has 456 publications in international academic journals, more than 150 research papers in domestic and over 190 articles in proceedings of International conferences with more than 10,000 citations.